Plant Cell 32 (12): 3902-3920 (2020)

Abscisic Acid-Triggered Persulfidation of Cysteine Protease ATG4 Mediates Regulation of Autophagy by Sulfide

Ana M. Laureano-Marín[a,1], Ángeles Aroca[a,1], M. Esther Pérez-Pérez[a], Inmaculada Yruela[b,c], Ana Jurado-Flores[a], Inmaculada Moreno[a], José L. Crespo[a], Luis C. Romero[a], Cecilia Gotor[a,2]

[a]Instituto de Bioquímica Vegetal y Fotosíntesis, Consejo Superior de Investigaciones Científicas and Universidad de Sevilla, Seville, Spain

[b]Estación Experimental de Aula Dei, Consejo Superior de Investigaciones Científicas, Zaragoza, Spain

[c]Group of Biochemistry, Biophysics and Computational Biology (BIFI-Unizar) Joint Unit to CSIC, Spain

[1]These authors contributed equally to this work

[2]Address correspondence to gotor@ibvf.csic.es.

Short title: ATG4 is a target of sulfide

The author responsible for distribution of materials integral to the findings presented in this article in accordance with the policy described in the Instructions for Authors (www.plantcell.org) is: Cecilia Gotor (gotor@ibvf.csic.es).

ABSTRACT

Hydrogen sulfide is a signaling molecule that regulates essential processes in plants, such as autophagy. In *Arabidopsis thaliana*, hydrogen sulfide negatively regulates autophagy independently of reactive oxygen species via an unknown mechanism. Comparative and quantitative proteomic analysis was used to detect abscisic acid-triggered persulfidation that reveals a main role in the control of autophagy mediated by cysteine protease AtATG4a. This protease undergoes specific persulfidation of Cys170 that is a part of the characteristic catalytic Cys-His-Asp triad of cysteine proteases. Regulation of the ATG4 activity by persulfidation was tested in a heterologous assay using the *Chlamydomonas reinhardtii* CrATG8 protein as a substrate. Sulfide significantly and reversibly inactivates AtATG4a. The biological significance of the reversible inhibition of the ATG4 by sulfide is supported by the results obtained in Arabidopsis leaves under basal and autophagy-activating conditions. A significant increase in the overall ATG4 proteolytic activity in Arabidopsis was detected under nitrogen starvation and osmotic stress and can be inhibited by sulfide. Therefore, the data strongly suggest that the negative regulation of autophagy by sulfide is mediated by specific persulfidation of the ATG4 protease.

INTRODUCTION

Hydrogen sulfide is currently recognized as a signaling molecule. In plant systems, H_2S is considered to be as important as NO and H_2O_2 and regulates essential processes of plant performance (Garcia-Mata and Lamattina, 2013; Calderwood and Kopriva, 2014; Jin and Pei, 2015; Gotor et al., 2017). Sulfide mediates tolerance against a range of plant stresses from heavy metal toxicity to salinity and drought to enhance plant viability (Gotor et al., 2019). Sulfide regulates critical processes, including autophagy (Alvarez et al., 2012; Gotor et al., 2013; Gotor et al., 2015; Laureano-Marin et al., 2016b; Laureano-Marin et al., 2016a) and the abscisic acid (ABA)-dependent stomatal movement (Jin et al., 2013; Scuffi et al., 2014; Papanatsiou et al., 2015; Scuffi et al., 2018).

Despite increasing evidence of the biological function of H_2S, there is a considerable lack of information on the mechanism of action of H_2S in particular physiological processes. The mechanism of action must be related to chemical reactivity of H_2S with other molecules. H_2S was suggested to coordinate the metal centers of metalloproteins (Vitvitsky et al., 2018) or act as a reductant of reactive oxygen species (Zaffagnini et al., 2019). A third mechanism of action of H_2S is based on its ability to modify the thiol group (-SH) of the cysteine residues in target proteins to form a persulfide group (-SSH) resulting in functional changes in the protein structure, activity, or subcellular localizations (Aroca et al., 2015; Aroca et al., 2017b). This posttranslational modification is called persulfidation (known previously as S-sulfhydration) and has been initially demonstrated in the mammalian (Mustafa et al., 2009; Paul and Snyder, 2012) and plant systems (Aroca et al., 2015; Aroca et al., 2017a) using specific labeling methods.

Our previous investigations in *Arabidopsis thaliana* demonstrated that hydrogen sulfide functions as a signaling molecule in the cytosol that negatively regulates autophagy (Alvarez et al., 2012; Gotor et al., 2013; Romero et al., 2013), which is a highly conserved process involving digestion of the cell contents for recycling and maintenance of cell homeostasis. Autophagy occurs at the basal levels in eukaryotic cells and is induced by internal or external perturbations. In plants, autophagy is involved in development, immune response, and senescence and is induced by stress conditions, including nutrient limitation and other abiotic stresses (Liu and Bassham, 2012; Pérez-Pérez et al., 2012; Masclaux-Daubresse et al., 2017; Ustun et al., 2017;

Marshall and Vierstra, 2018a). This catabolic process is characterized by *de novo* synthesis of autophagosomes in the cytosol, in which cytoplasmic materials to be recycled are sequestrated, transported, and released into the plant vacuole. Various receptors have been described to assist with specific cargo recruitment and degradation via selective autophagy. The core autophagy machinery is highly conserved in all studied eukaryotes, and involved proteins are referred to as autophagy-related (ATG). These ATG proteins include the ATG8 and ATG12 ubiquitin-like conjugation systems that catalyze the covalent attachment of ATG8 to the phospholipid phosphatidylethanolamine (PE), which is an essential adduct for the formation of autophagosomes (Mizushima et al., 2011). Before this conjugation, the C-terminal extension of newly synthetized ATG8 has to be cleaved by the Cys-type protease ATG4 to expose a highly conserved Gly, which is necessary for conjugation to PE. Additionally, ATG4 functions as a deconjugating enzyme that cleaves the amide bond between ATG8 and PE allowing the recycling of free ATG8 (Nair et al., 2012; Nakatogawa et al., 2012; Yu et al., 2012).

The role of sulfide as a repressor of autophagy is independent of nutrient conditions and specific tissues because sulfide inhibits autophagy in leaves under dark-induced carbon starvation (Alvarez et al., 2012) or in roots under nitrogen deprivation (Laureano-Marin et al., 2016a), and both conditions are unrelated to sulfur metabolism. A study aiming to decipher the mechanism of action of H_2S showed that it is independent of the formation of reactive oxygen species (ROS), such as hydrogen peroxide or superoxide anions, and therefore H_2S does not serve as a reducer in the regulation of autophagy (Laureano-Marin et al., 2016a). Interestingly, a comparative and quantitative proteomic analysis was performed to detect endogenous persulfidated proteins; the results indicated that at least 10% of the entire Arabidopsis proteome undergoes persulfidation under physiological conditions suggesting a widespread distribution of this posttranslational modification (Aroca et al., 2017a). Furthermore, persulfidation of various components of the ABA signaling pathway has been recently described as a specific mechanism of action by which H_2S controls the guard cell ABA signaling (Chen et al., 2020; Shen et al., 2020).

In this study, a comparative and quantitative proteomic analysis was used to detect persulfidated proteins in the leaves of Arabidopsis exogenously treated with ABA. Interestingly, comparison of the untreated and ABA-treated samples indicated that AtATG4a was the protein with the highest difference in the persulfidation level. We

then sought to determine whether persulfidation is the mechanism of the regulation of autophagy by sulfide in Arabidopsis under the stress conditions and to ascertain whether persulfidation regulates the activity of ATG4. To this aim, an enzymatic assay using *C. reinhardtii* CrATG8 as ATG4 substrate was developed. In-depth analysis of ATG4 proteolytic activity was performed *in vitro* and in a cell-free system using total extracts from Arabidopsis under basal or autophagy-activating conditions, including nitrogen limitation or osmotic stress. The results indicate that ATG4 is a specific target of persulfidation.

131

RESULTS

Autophagy induction by abscisic acid-triggered persulfide modification is mediated by AtATG4a regulation by hydrogen sulfide in Arabidopsis

Abscisic acid can trigger changes in hydrogen sulfide level and protein persulfide modification in the guard cells to modulate stomatal closure (Shen et al., 2020). To assess whether ABA also regulates protein persulfidation levels in the mesophyll cells, a sequential window acquisition of all theoretical spectra-mass spectrometry (SWATH-MS) quantitative approach was combined with the tag-switch method to measure protein persulfidation (Aroca et al., 2017a). Protein samples from three biological replicates (independent pools) of leaf tissue treated with ABA for 0 h (control sample), 3 h, and 6 h were isolated and subjected to the tag-switch procedure (Figure 1A). The proteins eluted from the streptavidin beads were digested, and the peptide solutions analyzed in two sequential steps: a shotgun data-dependent acquisition (DDA) approach to generate the spectral library and SWATH acquisition by the data-independent acquisition (DIA) method. In the first step, integration of the nine datasets resulted in identification of a total of 10,329 peptides (1% FDR and 90% confidence) and 1,434 unique proteins (1% FDR) that were used as a spectral library (Supplemental Dataset 1). In the second step, to quantify protein levels using SWATH acquisition, the same six biological samples were analyzed in two technical replicates by the DIA method using the LC gradient and LC-MS equipment employed in generation of the spectral library.

Therefore, six datasets were generated from the control and ABA-treated (for 3 and 6 h) samples to yield a total of 18 datasets used for the quantitative analysis. The fragment spectra were extracted for the eighteen runs, and 33,887 ion transitions, 4,871 peptides, and 1,157 proteins were quantified. Principal component analysis (PCA) of the protein sample subgroups revealed significant reproducible data between the replicates and differences between the ABA treatments (Figure 1B).

Comparison between the control (0 h) and the 3 h ABA treatment samples (0 h vs 3 h ABA; Supplemental Dataset 2) showed that 192 proteins were more abundant in the control samples with the fold change > 1.5 (p value < 0.05), and 242 proteins were less abundant with the fold change < 0.66 (p value < 0.05) (Supplemental Dataset 3) (Figure 1C). Higher abundance of a protein in the control samples than that in the samples prepared after 3 h ABA treatment means that the protein is more persulfidated in the

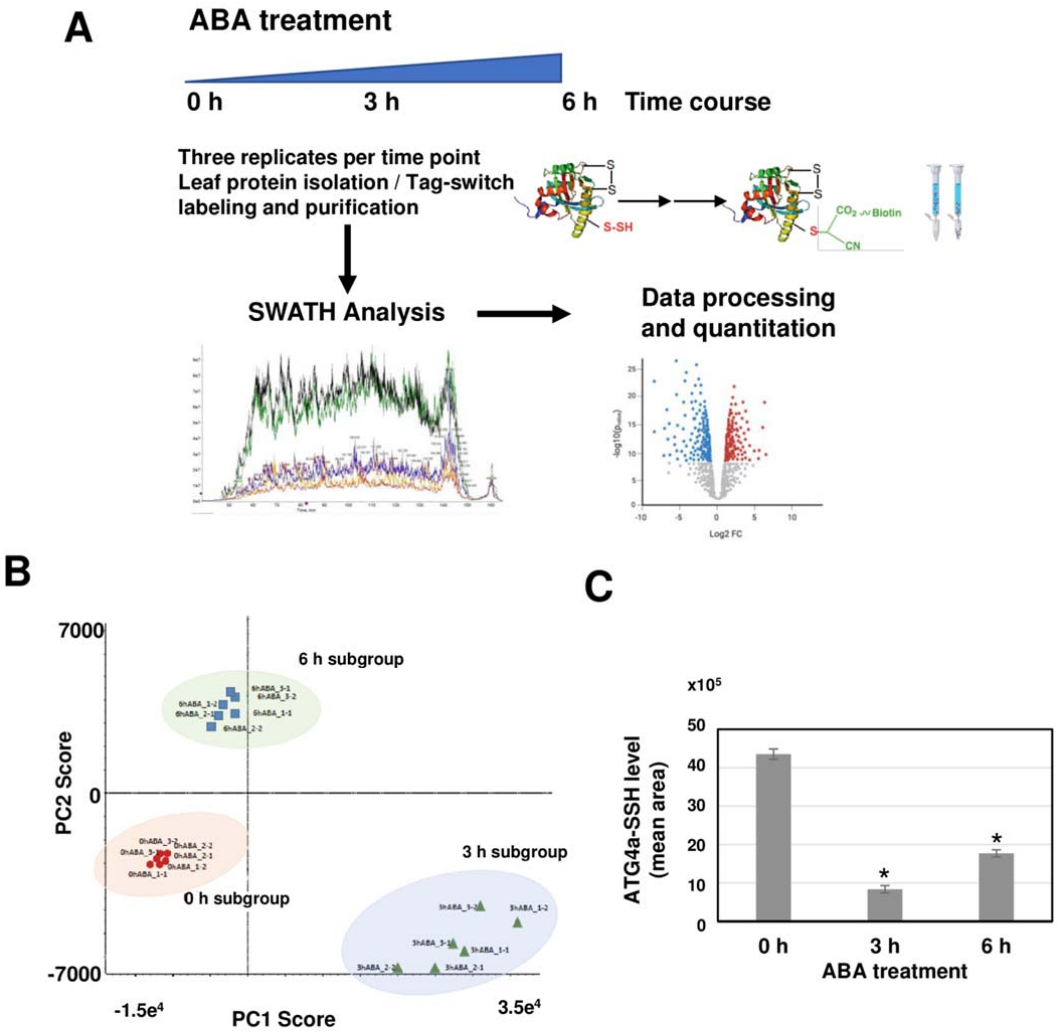

Figure 1. Proteomic analysis of protein persulfidation in response to ABA in mesophyll cells.
(A) Workflow of ABA leaf treatments followed by tag-switch protein labeling with CN-biotin, protein purification, and quantitative SWATH analysis of eluted proteins.
(B) PCA representation plot of the 18 samples after SWATH analysis. Score for PC1 (70 %) versus PC2 (9.9%), Pareto scaling.
(C) Level of persulfidated ATG4a after ABA treatments. Values represent the mean peak areas of extracted ion chromatogram of identified ATG4a peptides. *, $p<0.05$

control because the tag-switch labeling recovers more protein from the streptavidin column. Lower abundance in the control means that a protein is more persulfidated in the 3 h ABA samples.

A total of 192 proteins with reduced persulfidation level after 3 h of ABA treatment were analyzed based on their assigned functions and classified into 32 functional groups using the MapMan nomenclature (Thimm et al., 2004; Klie and Nikoloski, 2012) (Supplemental Table 1). The most numerous set corresponded to the general protein

group (bin 29) (Supplemental Table 2), which included 18.2% of the total identified proteins with 35 total elements, 29 of which are involved in protein amino acid activation (8 elements, tRNA ligases), protein synthesis (12 elements) and protein degradation (9 elements). The latter group included the Cys-type protease AtATG4a involved in autophagy, which showed the highest persulfidation change (5.20-fold change), and the S1 RNA-BINDING RIBOSOMAL PROTEIN 1 (3.69-fold change) that regulates seedling growth in the presence ABA or under abiotic stress conditions (Gu et al., 2015). Additional proteins involved in the regulatory process and with a reduction in their persulfidation levels included MAPK kinase 6 (MPK6, AT2G43790), tyrosine phosphatase 1 (PTP1, AT1G71860), glycine-rich protein 8 (GRP8, AT4G39260), and 9-cis-epoxycarotenoid dioxygenase 4 (NCED4, AT4G19170).

The quantitative analysis of the control and the 6 h ABA treatment samples (Supplemental Dataset 4) showed a reduction in the number of regulated proteins; only 120 proteins were more abundant in the control *versus* the ABA treatment samples with the fold change > 1.5 (p value < 0.05), and 198 proteins were less abundant with the fold change < 0.66 (p value < 0.05) (Supplemental Dataset 5) (Figure 1C).

Comparison of differentially regulated proteins at 3 and 6 h of ABA treatment showed that 42% of the proteins are regulated under both conditions and had different level of persulfidation. The cysteine protease AtATG4a showed a reduction in the level of persulfidation down to only 2.45-fold after 6 h of ABA treatment compared to that under the control conditions; this level was higher than that in the 3 h ABA treatment samples (Figure 1D). Therefore, persulfidation level of AtATG4a was transiently reduced after a short ABA treatment, and this reduction was very significant compared to the untreated control.

The proteomics data suggest that AtATG4a protease is differentially persulfidated depending on the treatment conditions, which may be related with the progress of autophagy. To prove this assumption, the regulation of autophagy by ABA treatments and the effects of sulfide under these conditions were analyzed. Arabidopsis seedlings expressing GFP-ATG8e fusion protein (Xiong et al., 2007) were treated with 50 μM ABA for 3 and 6 h and subjected to additional treatment of 200 μM NaHS for 1 h. Total protein extracts were obtained, and immunoblot analysis was performed using anti-GFP antibodies to detect free GFP and the GFP-ATG8e fusion protein (Figure 2A). A clear increase in the free GFP protein level in ABA-treated seedlings was detected compared

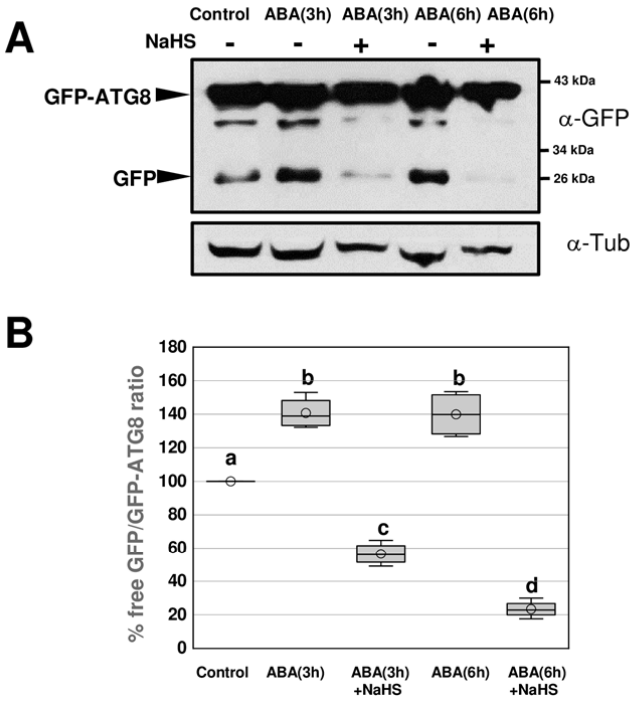

Figure 2. Effect of sulfide on autophagy induced by ABA treatment.
(A) Immunoblot analysis of GFP-ATG8e fusion protein. One-week-old seedlings expressing GFP-ATG8e fusion protein were transferred to liquid MS media and were not treated (control) or treated with 50 μM ABA for 3 and 6 h and then 200 μM NaHS for 1 h. Total protein extracts were prepared and subjected to SDS-PAGE and immunoblot analysis with anti-GFP antibodies. Anti-tubulin antibodies were used as the protein-loading control.
(B) Quantification of the free GFP/GFP-ATG8 ratio. For each condition, the levels of free GFP and GFP-ATG8e fusion protein were quantified in a less exposed blot shown in Supplemental Figure 6. The value of 100% was assigned to the free GFP/GFP-ATG8 ratio of the control sample. Data are from three independent experiments and evaluated by two-factor ANOVA. Same letters indicate no significant differences. $P < 0.05$.

with the control and a significant reduction in the GFP accumulation after the additional sulfide treatment was observed resulting in protein levels lower than those detected in the control. Quantification of the ratio free GFP/GFP-ATG8 under each condition showed that ABA induced the autophagic flux and that this ABA-induced autophagy was repressed by NaHS (Figure 2B). These findings and the proteomic data suggest that sulfide is a negative regulator of bulk autophagy independently of the condition used to induce this catabolic process, including at least nutrient limitation (Alvarez et al., 2012; Laureano-Marin et al., 2016a) and ABA-dependent stress (this study). Furthermore, persulfidation appears to be the mechanism of action of sulfide and the AtATG4a protease may be one of the specific targets.

Persulfidation of AtATG4a at the Cys170

To demonstrate the persulfidation-based modification of Cys residues in AtATG4a, recombinant protein was purified, subjected to the tag-switch procedure, and analyzed by immunoblotting using anti-biotin antibodies (Aroca et al., 2017a). A biotin-labeled protein band corresponding to AtATG4a was clearly detected by the antibody. Moreover, when AtATG4a was pretreated with DTT to reduce the persulfide residues, the biotin-labeled protein bands were not detected (Figure 3A). These results clearly indicate that AtATG4a undergoes persulfidation *in vitro*. To identify the Cys residue that can be modified by persulfidation, recombinant AtATG4a was analyzed by liquid chromatography (LC)-tandem mass spectrometry (MS/MS). The protein was digested with trypsin under nonreducing conditions in the absence of alkylating agents to avoid the reduction or modification of the persulfide residues. The digested peptides were analyzed to detect a 32 Da molecular mass increase in the fragmentation spectrum. The identified peptides included DTTYTSDVNWGCMIR that showed a persulfidation modification of Cys170 (Figure 3B). AtATG4a protein was identified with a sequence coverage of 97%, and no other persulfidated peptides were detected despite the presence of other eleven Cys residues in the primary structure (Figure 3C). Cys170 is located in the highly conserved catalytic site of ATG4 proteins from various organisms (Satoo et al., 2009; Perez-Perez et al., 2014; Perez-Perez et al., 2016) suggesting that the modification by persulfidation may have an important impact on the AtATG4a proteolytic activity and biological function.

In Vitro Processing of CrATG8 by AtATG4a

To determine whether modification of AtATG4 by persulfidation has an effect on its biological activity, an *in vitro* assay using CrATG8 from *C. reinhardtii* as a substrate was established (Perez-Perez et al., 2010). CrATG8 was previously used to monitor the activity of yeast ATG4 (Perez-Perez et al., 2010; Perez-Perez et al., 2014). ATG4 processes ATG8 at a conserved glycine residue located at the C-terminus of the protein (Kirisako et al., 2000). Arabidopsis contains nine different ATG8 isoforms, none of which has more than five amino acid residues after the conserved glycine (Doelling et al., 2002). In contrast, CrATG8 harbors a 14-amino acid extension after the glycine, and CrATG8 processing can be easily monitored by Coomassie Blue-stained SDS-PAGE

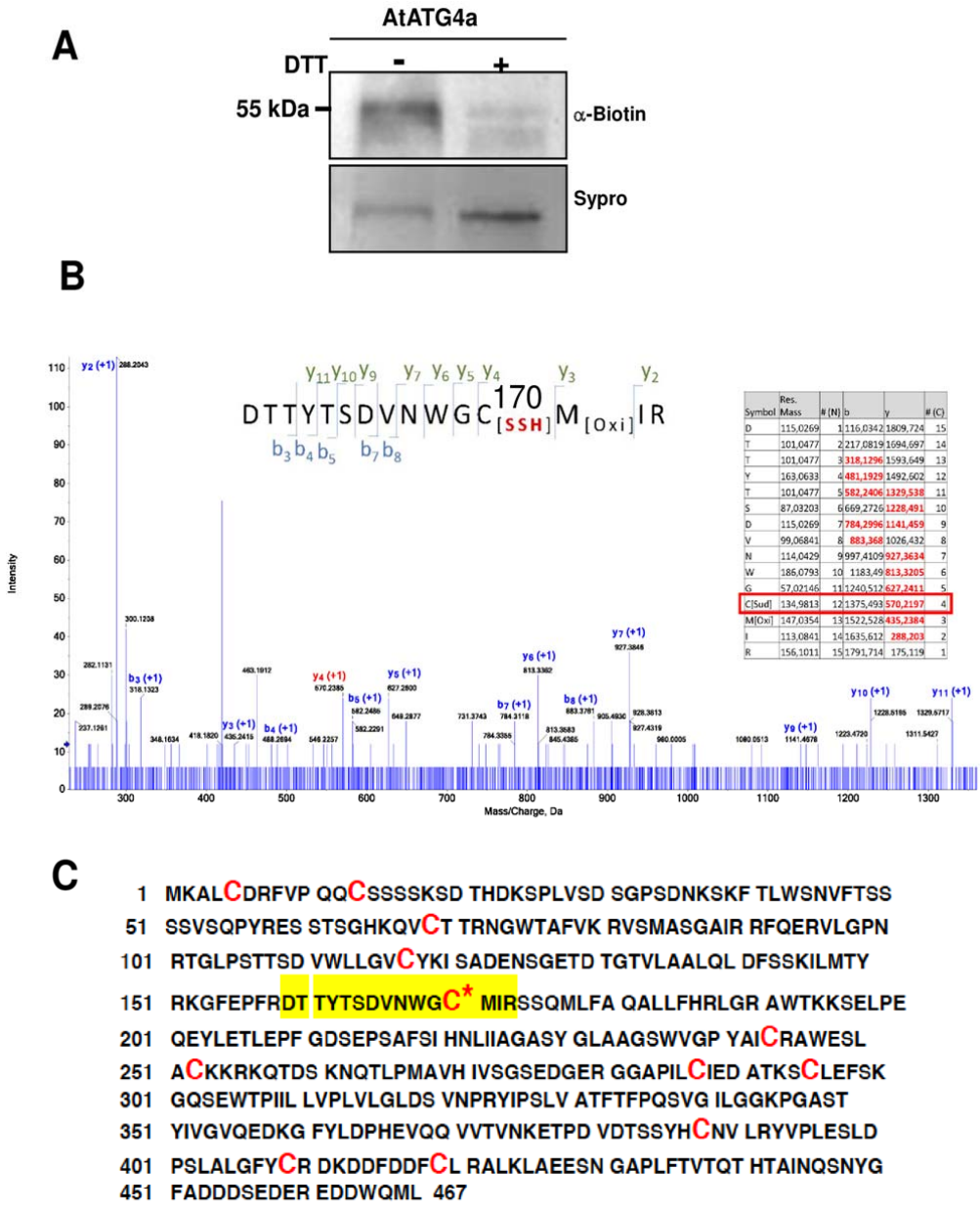

Figure 3. Persulfidation of Arabidopsis AtATG4a
(A) Immunoblot analysis of persulfidated AtATG4a. Purified recombinant AtATG4a was treated in the absence (-) or in the presence of 50 mM DTT (+) for 30 min at 4ºC, dialyzed, and subjected to the tag-switch labeling as described in the Methods. Then, the proteins were subjected to immunoblot analysis using anti-biotin antibodies. Sypro Ruby fluorescent staining is shown as the protein loading control.
(B) Analysis of AtATG4a using mass spectrometry. LC-MS/MS analysis of a tryptic peptide of AtATG4a containing Cys170. The table inside the spectrum contains the predicted ion types for the modified peptide, and the ions detected in the spectrum are highlighted in red.
(C) AtATG4a protein sequence identified with 97% coverage. The peptide containing persulfidated Cys170 is highlighted in yellow and all the Cys residues are red.

due to differences in mobility between the unprocessed and processed CrATG8 forms (Supplemental Figure 1). When purified AtATG4a was incubated with CrATG8 in the

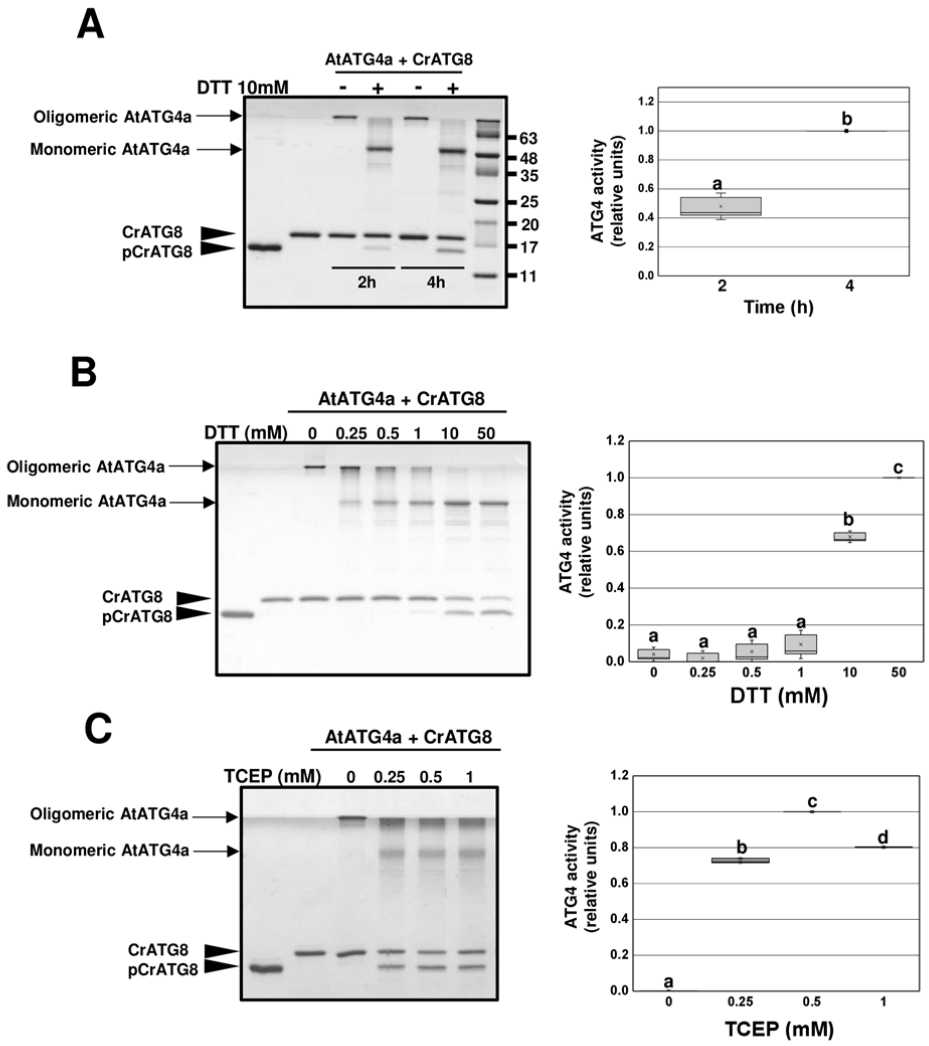

Figure 4. Arabidopsis ATG4a cleaves Chlamydomonas ATG8.
ATG4 activity of the recombinant AtATG4a was assayed by monitoring the cleavage of CrATG8 from the unprocessed (CrATG8) to processed (pCrATG8) forms (indicated by arrowheads) using SDS-PAGE followed by Coomassie Blue staining and quantification of protein band intensities. The ATG4 activity (relative units) was determined as the ratio of the band intensity of the processed CrATG8 to the sum of the intensities of the unprocessed and processed CrATG8. Activity value of 1 corresponds to the maximum. Processed pCrATG8 (lane 1) and unprocessed CrATG8 (lane 2) were loaded as controls. Representative images are shown. Data are from three independent experiments and evaluated by two-factor ANOVA. Same letters indicate no significant differences. $P < 0.05$.
(A) Effect of incubation time. AtATG4a was incubated with CrATG8 in the absence or in the presence of 10 mM DTT for the indicated times.
(B) Effect of DTT concentration. AtATG4a was incubated with CrATG8 in the absence or in the presence of increasing concentrations of DTT for 4 h.
(C) Effect of TCEP concentration. AtATG4a was incubated with CrATG8 in the absence or in the presence of increasing concentrations of TCEP for 4 h.

presence of DTT, the processed protein with the same mobility as a truncated form lacking the last 14 amino acids ($CrATG8^{G120}$, referred to as pCrATG8) was detected (Figure 4A). Therefore, AtATG4a was active and was able to process CrATG8 at its C-

terminal Gly validating the ATG4 processing activity assay. The results indicated that AtATG4a activity was increased in a time-dependent manner and required a reducing agent to adopt the monomeric form required for the activity (Figure 4A), as described previously in other systems (Perez-Perez et al., 2010). To analyze the effect of a reducing agent on AtATG4a activity, the *in vitro* assay in the presence or in the absence of different DTT or TCEP concentrations was performed. In the absence of DTT and TCEP, recombinant AtATG4a was in an oligomeric form that was retained in the upper part of the acrylamide gel. Increasing concentrations of the reducing agent enhanced the monomerization of recombinant AtATG4a and consequently the processing of CrATG8 by AtATG4a (Figure 4B and 4C). Therefore, properties of Arabidopsis ATG4a were similar to those of the Chlamydomonas and yeast ATG4 (Perez-Perez et al., 2014; Perez-Perez et al., 2016). Interestingly, TCEP was more efficient than DTT in the activation of CrATG8 cleavage, showing the maximum level of ATG4 activity at 0.5 mM TCEP while two orders of magnitude higher DTT concentration was required for optimal activity (Figure 4B and 4C).

Sulfide inhibits the proteolytic activity of AtATG4a

A suitable ATG4 enzyme activity assay was developed and used to study whether persulfidation plays a role in the regulation of this activity. Thus, purified recombinant AtATG4a was pretreated with TCEP to produce an active enzyme and then incubated with increasing concentrations of NaHS as a sulfide donor. The ATG4 activity-dependent CrATG8 processing was determined using the Coomassie-stained gel method (Figure 5A). An increase in the accumulation of the unprocessed CrATG8 form was detected when AtATG4a was incubated in the presence of NaHS at a concentration as low as 0.1 mM. ATG4 activity was determined as the ratio of the band intensity of the processed CrATG8 to the sum of the intensities of the unprocessed and processed CrATG8; the data indicate that 0.1 mM NaHS significantly inhibits the ATG4 activity to approximately 40% of the activity in the absence of sulfide (Figure 5B). Interestingly, analysis of the aggregation state of AtATG4a in the presence of the sulfide donor demonstrated that NaHS has different effects on monomerization and activity of AtATG4a (Figure 5C). Sulfide did not promote the oligomerization of the active monomeric AtATG4a to the same extent as it inhibited ATG4 proteolytic activity under the conditions used in the assays. Concentrations of NaHS from 0.1 to 0.5 mM did not

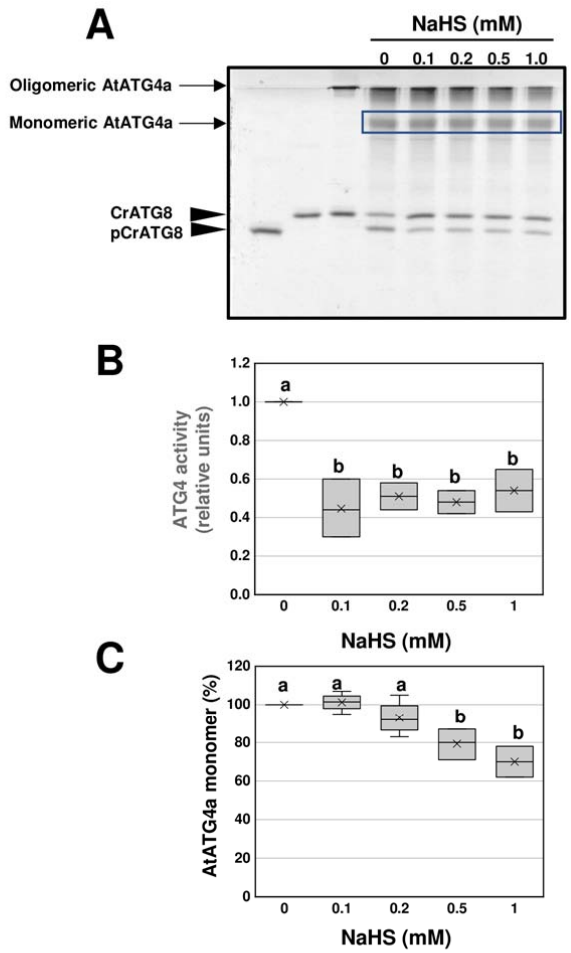

Figure 5. Effect of NaHS on AtATG4a enzyme activity.
(A) AtATG4a was incubated with 0.5 mM TCEP for 2 h and treated in the absence or the presence of indicated concentrations of NaHS for 1 h. Then, CrATG8 was added to the incubation mixture, and ATG4 activity was monitored after 4 h using Coomassie-stained gels as described in the Methods. All procedures were performed at 25ºC. Lane 1 and 2, unprocessed and processed CrATG8, respectively. Lane 3, AtATG4a incubated with CrATG8 in the absence of TCEP and of NaHS. Lanes 4-8, TCEP-pretreated reduced AtATG4a incubated with CrATG8 in the presence of increasing concentrations of NaHS (from 0 to 1 mM). A representative image is shown.
(B) Quantification of ATG4 activity (relative units) determined as the ratio of the band intensity of the processed CrATG8 to the sum of the intensities of the unprocessed and processed CrATG8. A value of 1 corresponds to AtATG4a in the absence of NaHS (lane 4).
(C) Quantification of the protein band intensity corresponding to the monomeric AtATG4a form marked by a rectangle in A. A value of 100% corresponds to AtATG4a in the absence of NaHS (lane 4).
Data are from three independent experiments and evaluated by two-factor ANOVA. Same letters indicate no significant differences. $P < 0.05$

significantly increase the abundance of high molecular weight and inactive oligomers of AtATG4a (Figure 5C). These results indicate that sulfide donor inhibits AtATG4a activity but does not directly influence the aggregation state of the protein in contrast to the effect of DTT or thioredoxin on yeast and *C. reinhardtii* ATG4 proteins (Perez-Perez et al., 2014; Perez-Perez et al., 2016).

295 Recent studies have questioned whether NaHS can be the sulfurating molecule
296 instead of the proposed polysulfide and persulfide molecules. These molecules contain
297 sulfane sulfur, the form of sulfur (S^0) with the ability to reversibly attach to other sulfur
298 atoms. Most of the reported biological activity associated with sulfide may be due to
299 persulfides, which are considered responsible for the intracellular signal transduction
300 through persulfidation in the living body (Toohey, 2011; Ida et al., 2014; Mishanina et
301 al., 2015). Thus, assays similar to those described above were performed using various
302 concentrations of polysulfide Na_2S_4 used as a sulfur donor. Our results indicated that
303 polysulfide inactivates AtATG4a more efficiently than NaHS (Figure 6A and 6B).
304 Concentrations of Na_2S_4 three orders of magnitude (10-50 μM) lower than those of
305 NaHS were necessary to achieve a similar inhibition, and complete inactivation of the
306 enzyme was observed at 100 μM Na_2S_4. Furthermore, polysulfides were more active in
307 promoting the aggregation state of AtATG4a, and the differences in the effects on
308 activity and oligomerization were not as pronounced as those observed with NaHS
309 (Figure 6C).
310 Collectively, our results indicate that sulfide can inhibit the ATG4 proteolytic
311 activity and that this inhibition is independent on the ATG4 aggregation state, at least at
312 low concentrations of sulfurating species. Our results also suggest that this inhibitory
313 effect is mediated by specific persulfidation of the catalytic Cys170 residue. Site-
314 directed mutagenesis of this catalytic cysteine inactivates ATG4 activity in all tested
315 systems and conditions (Scherz-Shouval et al., 2007; Shu et al., 2010; Perez-Perez et al.,
316 2014; Perez-Perez et al., 2016), and therefore the mutant enzyme cannot be used to test
317 the inhibitory effect of sulfide.
318 To examine the impact of posttranslational modification of Cys170 by persulfidation
319 on the interaction between AtATG4a and its substrate AtATG8a, 3D homology
320 modelling was performed using the structure of the *Homo sapiens* HsATG4b-LC3
321 complex (Satoo et al., 2009). AtATG4a shares up to 33.4% sequence identity with
322 HsAtg4B (E-value $7.3x10^{-90}$) and AtATG8a shares up to 59.4% sequence identity with
323 HsLC3 (E-value $1.8x10^{-40}$) with conserved residues covering the whole sequence.
324 Persulfidation of Cys170 in the AtATG4a-AtATG8a protein complex caused
325 conformational changes and intramolecular rearrangements of the catalytic site (Figure
326 7A) influencing substrate recognition. Addition of the –SH group to Cys170 induced an
327 unfavorable steric effect particularly affecting the His366 residue since the imidazole

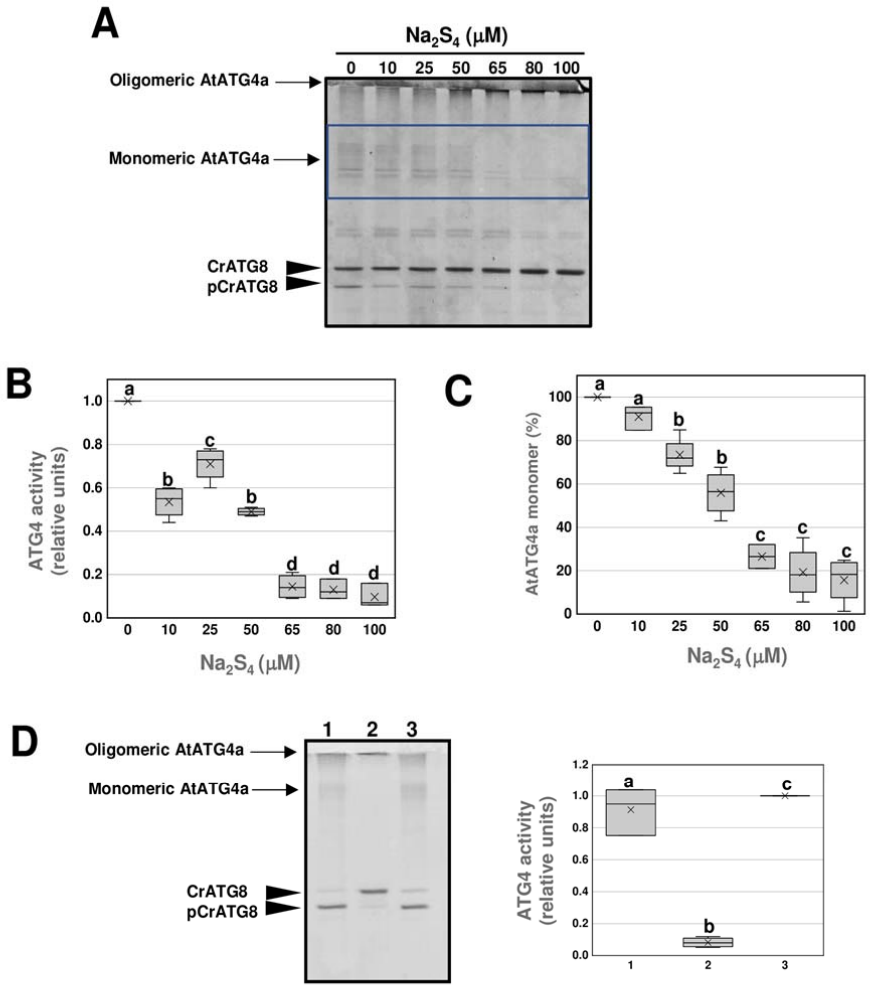

Figure 6. Effect of polysulfides on AtATG4a enzyme activity.
(A) AtATG4a was incubated with 0.5 mM TCEP for 2 h and subsequently treated in the absence or in the presence of indicated concentrations of Na_2S_4 for 1 h. Then, CrATG8 was added to the incubation mixture, and ATG4 activity was monitored after 4 h using Coomassie-stained gels as described in Methods. All procedures were performed at 25ºC. A representative image is shown.
(B) Quantification of ATG4 activity (relative units) determined as the ratio of the band intensity of the processed CrATG8 to the sum of the intensities of the unprocessed and processed CrATG8. A value of 1 corresponds to AtATG4a treated in the absence of Na_2S_4 (lane 1).
(C) Quantification of the protein band intensity corresponding to the monomeric AtATG4a form marked by a rectangle in A. A value of 100% corresponds to AtATG4a treated in the absence of Na_2S_4 (lane 1).
(D) Reversibility of the effect. AtATG4a was first incubated with 0.25 mM TCEP for 2 h (lane 1) and treated with 100 mM Na_2S_4 for 1 h (lane 2) and 1 mM TCEP for 1 h (lane 3). ATG4 activity was monitored using Coomassie-stained gels. The experiment was performed at least three times and a representative image used for the quantification of the activity is shown.
Data are from three independent experiments and evaluated by two-factor ANOVA. Same letters indicate no significant differences. $P < 0.05$

328 Cδ2 and Nε2 atoms are 2.9 Å and 3.4 Å from the S atom of Cys170, respectively. The
329 additional sulfur and hydrogen atoms have a covalent radius of 1.02 Å and 0.37 Å,
330 respectively (Figure 7B). Therefore, this cysteine modification can inhibit the activity of

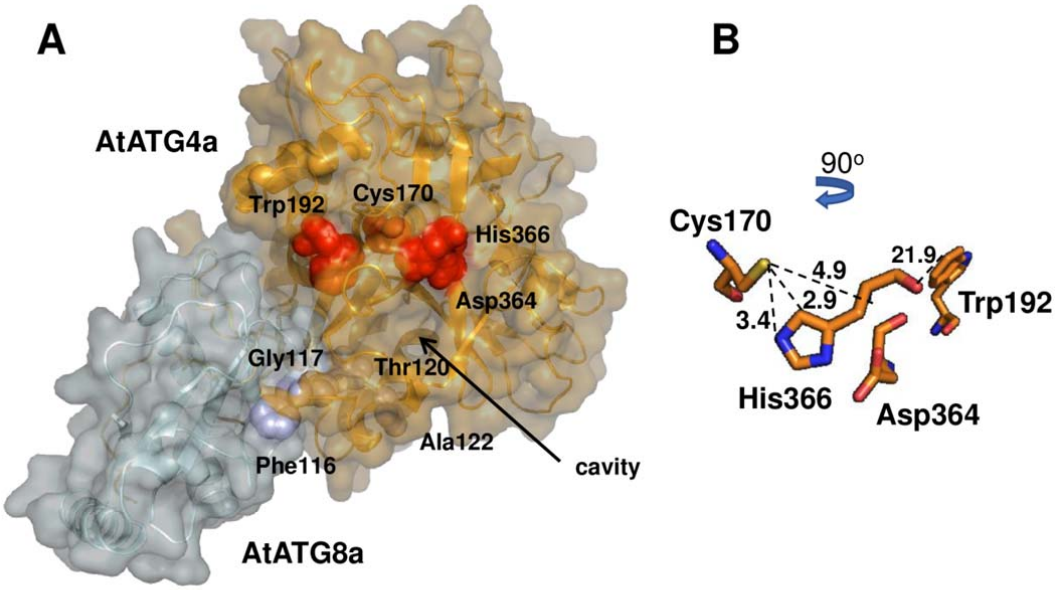

Figure 7. Predicted structure of the AtATG4a-AtATG8a complex.
(A) 3D modelling of the AtATG4a-AtATG8a complex based on the structure of the HsAtg4B-LC3 protein complex (PDB ID: 2Z0E). The AtATG8 protein sequence (Q8LEM4 in UniProtkB) corresponds to the splice variant 1. Surface representation of the protein complex and the equivalent residues surrounding the catalytic cavity Cys170, Trp192, Asp364, and His366 in AtATG4a (red) and Phe116, Gly117, Thr120, and Ala122 in AtATG8a (blue) are shown in the structural models.
(B) Zoomed view of the putative conformation of the active site showing the spheres corresponding to the position and distance (Å) of catalytic residues Cys170, Trp192, Asp364, and His366 in AtATG4a.

the plant AtATG4a protein. Interestingly, the simulation of surface electrostatic potential reveals the differences between HsATG4b-LC3 and AtATG4a-AtATG8a protein complexes; specifically, the electrostatic potential surface around the catalytic site of the human complex is more electronegative compared to that of the Arabidopsis complex (Supplemental Figure 2). However, cysteine persulfidation does not perturb the charge, since the additional –SH group is a neutral contribution. A closer look at the catalytic cavity region suggests that it is somewhat smaller and less exposed to the solvent in Arabidopsis compared to the human homologue likely hampering the accessibility of the substrate. Overall, these data suggest that inhibition of the processing activity of Arabidopsis AtATG4a may be due to a conformational change of the catalytic site induced by persulfidation.

Endogenous Arabidopsis ATG4 processes CrATG8 for conjugation

Our results indicate that sulfide can regulate ATG4 proteolytic activity through persulfidation of a specific cysteine residue. This conclusion is based on *in vitro* experiments. If sulfide has a biological role in the control of ATG4 activity in living plants, the inhibitory effect of sulfide should be reversible. To explore this hypothesis, active AtATG4a was inhibited by a high concentration of Na_2S_4 to promote complete inactivation and to determine the extent of reversion by reduction of all persulfide residues with TCEP. The reactivation of AtATG4a was monitored as the ratio of the protein band intensities of unprocessed and processed CrATG8 (Figure 6D). The results clearly confirm that the inhibition of ATG4 proteolytic activity by sulfide is reversible, suggesting that it may play a role in the control of ATG4 *in vivo*.

To determine whether sulfide regulation of ATG4 also occurs *in vivo*, ATG4 enzyme activity was detected in Arabidopsis leaves using the addition of exogenous CrATG8 to leaf protein extracts. Immunoblot analysis using antibodies against CrATG8 indicated that CrATG8 was efficiently processed by incubation with Arabidopsis leaf protein extracts (Figure 8A, right part). To confirm the specificity of the CrATG8 cleavage assay, Arabidopsis leaf protein extracts were incubated with a mutant of CrATG8 with conserved Gly-120 replaced by Ala (G120A). This CrATG8 mutant is not processed by ATG4 (Perez-Perez et al., 2010; Perez-Perez et al., 2016). When G120A was used as the substrate, the processed form was not detected, demonstrating the specificity of the endogenous ATG4 activity in Arabidopsis (Figure 8A, left part). Moreover, in addition to full-length and processed CrATG8, the antibodies specifically recognized other bands with faster mobility than pCrATG8 (Figure 8, asterisks). These bands were exclusively detected when wild type CrATG8, but not the G120A mutant, was used in the assay and they apparently correspond to the conjugated form of CrATG8 protein, as demonstrated previously in Chlamydomonas (Perez-Perez et al., 2010). Incubation of the Arabidopsis protein extract with the processed form of the CrATG8 (pCrATG8), which does not require cleavage by ATG4 and can be conjugated to PE (Supplemental Figure 3), confirmed that the faster mobility bands correspond to lipidated forms. The antibodies detected mainly an intense protein band that was progressively accumulated with incubation time and fully lipidated at the shortest time of incubation with the extracts under autophagy-activating conditions induced by nitrogen deficiency (Supplemental Figure 3). Therefore, our data demonstrated that the Arabidopsis protein extracts contain all the active proteins required for the conjugation of ATG8 and efficiently

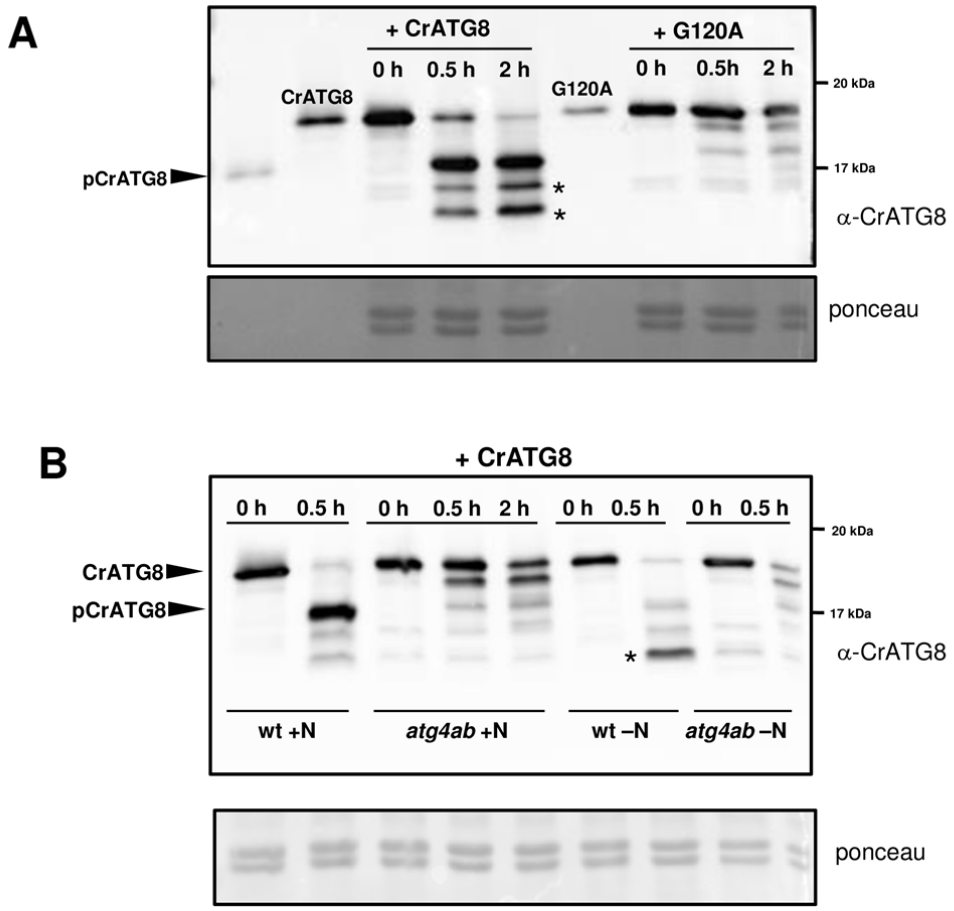

Figure 8. Cleavage and conjugation of Chlamydomonas ATG8 by Arabidopsis proteins.
(A) ATG4 proteolytic activity in wild-type Arabidopsis leaves. Arabidopsis protein extracts prepared from leaves of wild-type seedlings grown for 11 days on MS medium were incubated with CrATG8 or site-directed mutant G120A proteins at 25ºC for the indicated times, and ATG4 activity was monitored as the cleavage of the ATG8 forms to the processed (pCrATG8) forms by immunoblotting analysis with anti-CrATG8. Processed pCrATG8 (lane 1), unprocessed CrATG8 (lane 2), and site-directed mutant G120A (lane 6) were loaded as controls.
(B) ATG4 proteolytic activity in the Arabidopsis *atg4ab* mutant. Arabidopsis protein extracts were prepared from the leaves of wild-type and *atg4ab* double mutant seedlings grown for 7 days on the MS medium and transferred to the same medium (+N) or to a nitrogen-deficient medium (-N) for additional 4 days. The protein extracts were incubated with CrATG8 at 25ºC, and ATG4 activity was monitored after 0, 0.5, or 2 h, as indicated by immunoblotting analysis with anti-CrATG8.
The arrowheads show the unprocessed CrATG8 and processed pCrATG8 protein bands, and the asterisks indicate faster-mobility protein bands. Ponceau staining is shown as the protein loading control of the Arabidopsis extract.

recognize CrATG8, thus validating the results of the ATG4 activity assay in the cell-free total extract.

To confirm the conclusion that Arabidopsis ATG4 proteins catalyze the processing of CrATG8 in the cell-free total extract assay, the ATG4 enzyme activity of the Arabidopsis protein extracts prepared from the *atg4ab* double-mutant seedlings was

assayed (Supplemental Figure 4) (Yoshimoto et al., 2004; Chung et al., 2010). When CrATG8 was incubated with the Arabidopsis *atg4ab* protein extract, the processed form of CrATG8 was not detected even after extended incubation. Similarly, when protein extracts were prepared from nitrogen-limited seedlings, the immunoblot analysis revealed a prominent protein band corresponding to the lipidated form of CrATG8 only in the presence of protein extracts form wild-type plants but not from the *atg4ab* mutant (Figure 8B).

Therefore, our data show that endogenous Arabidopsis ATG4 proteins recognize the cleavage site of the Chlamydomonas ATG8 substrate, which is efficiently processed in the cell-free enzymatic assay.

Sulfide reversibly inhibits the ATG4 activity in Arabidopsis seedlings

The effect of a sulfurating species on endogenous Arabidopsis ATG4 proteins was investigated to confirm the results obtained in *in vitro* analysis. Leaf protein extracts were treated with polysulfide, and CrATG8-processing activity was compared with that in the untreated extract. A pronounced decrease in the ATG4 activity was observed when the Arabidopsis extract was pretreated with Na_2S_4 (Figure 9A). Additionally, treatment of the Arabidopsis leaf protein extract with the alkylating agent iodoacetamide inhibited ATG4 activity as expected because ATG4 is a Cys protease and its activity is dependent on the catalytic Cys; this effect was similar to the effect of polysulfide (Figure 9A, left panel). Thus, these findings strongly suggest that sulfide negatively regulates ATG4 activity *in vivo*, at least the cleavage activity of the C-terminal extension of ATG8. Reversibility of the inhibitory effect of polysulfide was also analyzed. When the polysulfide-incubated Arabidopsis extract was treated with TCEP as a reducing agent to reduce the persulfide-modified cysteine residues in the protein extract, a significant difference in the activity was detected compared with that in the polysulfide-treated extract (Figure 9A, right panel). When the extract was incubated with Na_2S_4, the processed CrATG8 form was barely detected; however, incubation with TCEP significantly increased the abundance of this band, suggesting that sulfide may inhibit Arabidopsis ATG4 activity in a reversible manner.

To characterize the inhibition of ATG4 proteolytic activity by sulfide, the effect of polysulfide on the ATG4 activity was assayed under basal and autophagy-inducing conditions. Two different established conditions of autophagy induction were tested:

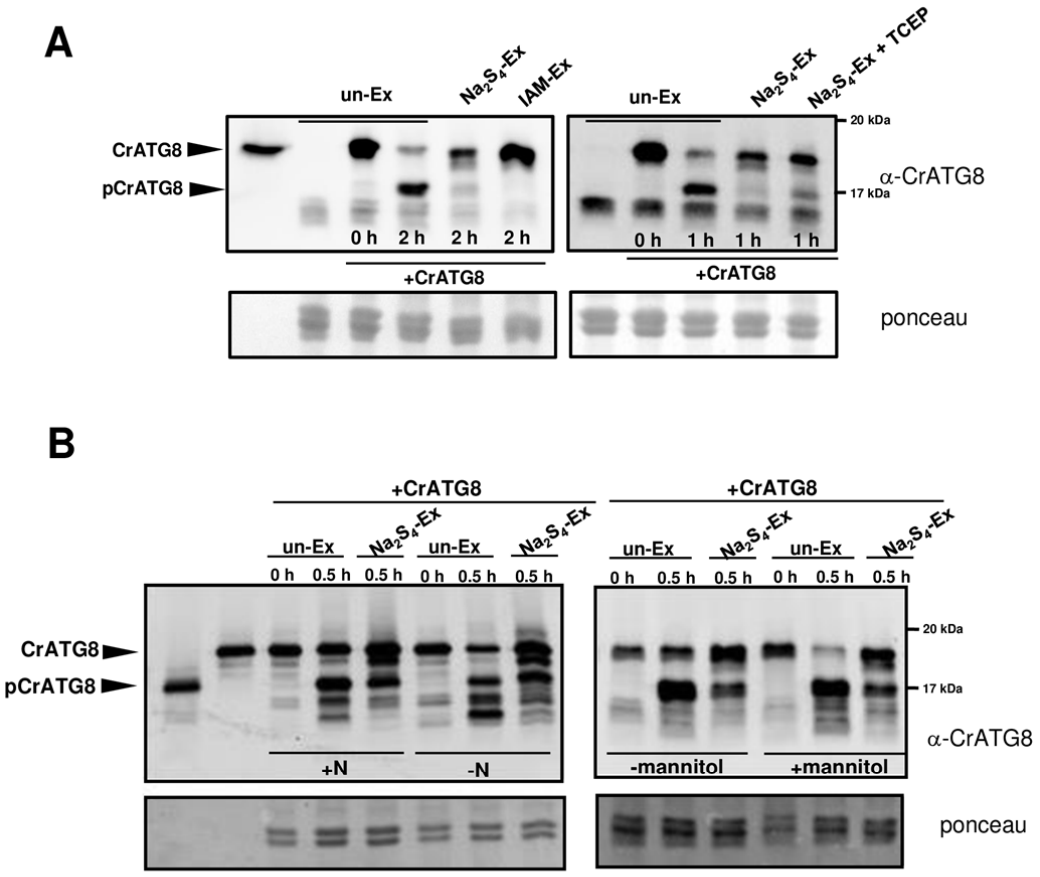

Figure 9. Sulfide inhibits the endogenous proteolytic activity of Arabidopsis ATG4.
(A) Effect of polysulfides on endogenous enzyme activity of Arabidopsis ATG4. Arabidopsis protein extracts (Ex) were prepared from the leaves of seedlings grown for 11 days on the MS medium. The extracts were treated in the absence (un-Ex) and in the presence of 200 μM Na_2S_4 (Na_2S_4-Ex), or 20 mM iodoacetamide (IAM-Ex) for 30 min, or in the presence of 200 μM Na_2S_4 for 30 min and 1 mM TCEP for 30 min (Na_2S_4-Ex + TCEP). Then, CrATG8 was added to the incubation mixture, and ATG4 proteolytic activity was monitored. Lane 1, unprocessed CrATG8.
(B) Sulfide reverts the endogenous enzyme activity of Arabidopsis ATG4 under autophagy-induced conditions. Arabidopsis protein extracts were prepared from the leaves of seedlings grown for 7 days on the MS medium and transferred to the same medium (+N) or to a nitrogen-deficient medium (-N) (left panel); or transferred to the same medium (-mannitol) or to same medium containing 300 mM mannitol (+mannitol) (right panel) for additional 4 days. The extracts were treated in the absence (un-Ex) or in the presence of 200 μM Na_2S_4 for 30 min (Na_2S_4-EX); CrATG8 was added to the incubation mixture and ATG4 activity monitored. Lane 1, processed pCrATG8 and lane 2, unprocessed CrATG8.
The ATG4 activity was monitored at the indicated times by immunoblotting analysis with anti-CrATG8. All procedures were performed at 25ºC. Ponceau staining is shown as the protein loading control.

417 nitrogen deficiency, which has been extensively characterized previously (Doelling et
418 al., 2002; Hanaoka et al., 2002; Xiong et al., 2005; Phillips et al., 2008; Guiboileau et
419 al., 2013; Laureano-Marin et al., 2016aa), and osmotic stress (Liu et al., 2009) imposed

by the addition of mannitol to the growth medium, which induces ABA-dependent signaling pathway. The processed form of CrATG8 was detected in total extracts under the control and autophagy-activating conditions, and sulfide inhibited endogenous ATG4 activity under both conditions (Figure 9B). The faster-mobility protein band corresponding to the lipidated form of CrATG8 was more prominent under nitrogen limitation than osmotic stress; however, sulfide treatment decreased the accumulation of the conjugated forms of CrATG8 under both conditions.

429

DISCUSSION

Accumulating evidence emphasizes the importance of autophagy in plant growth and development. This catabolic process is highly dynamic and occurs at the basal levels to maintain cellular homeostasis during growth; however, autophagy is fine-tuned to adjust plant metabolism to internal and external perturbations. Various regulators of autophagy have been identified in plant systems, such as energy sensor Snf1-related protein kinase 1 (SnRK1), target of rapamycin (TOR) kinase, the TOR downstream substrate ATG1 kinase complex, and the ER stress sensor inositol-requiring enzyme-1 (IRE1) (Marshall and Vierstra, 2018b; Soto-Burgos et al., 2018).

Other regulators of autophagy, such as hydrogen sulfide, have been identified although the details of the molecular mechanism of action of these regulators remain poorly understood. In the animal systems, interactions of sulfide with autophagy have been described in various pathologies; depending on the disease, sulfide can either suppress or activate autophagy. In all cases, hydrogen sulfide has protective effects (Sen, 2017; Wang et al., 2017; Wu et al., 2018). Despite substantial progress, the exact mechanism of autophagy regulation by sulfide in mammals remains unknown. In plants, particularly in Arabidopsis, the interplay between sulfide and autophagy has been shown, and progress in understanding of the mechanism has been obtained. Hydrogen sulfide generated in the cytosol functions as a signaling molecule negatively regulating autophagy independently of the nutritional conditions. Furthermore, sulfide was shown to repress autophagy via a mechanism that is independent of redox conditions (Alvarez et al., 2012; Laureano-Marin et al., 2016a).

Sulfur and autophagy are also linked by the mechanism of Arabidopsis sensing of the sulfur-containing amino acid cysteine. Two different pathways have been identified for sensing of its carbon/nitrogen precursor and its sulfur precursor. The sulfur precursor is transduced to TOR by downregulation of glucose metabolism; therefore, sulfide increases glucose levels and TOR kinase activity, downregulating autophagy (Dong et al., 2017). This study demonstrated that cytosolic sulfide is not the signal responsible for the regulation but does not exclude chloroplast sulfide as the signaling molecule. In fact, a proteomic study showed that other sulfurating species in addition to the cytosolic sulfide can be responsible for regulation of diverse biological processes (Aroca et al., 2017a).

The data of the present study emphasize sulfide regulation of autophagy. Our findings indicate that ABA activates autophagy and hydrogen sulfide downregulates this catabolic process. A link between autophagy and ABA was previously described through the Arabidopsis multistress regulator TSPO, a tryptophan-rich sensory protein-related. ABA induces TSPO as a heme scavenger, which binds the excessive or deleterious heme and then is targeted for degradation through autophagy (Vanhee and Batoko, 2011; Vanhee et al., 2011). Other connections between autophagy and ABA signaling via TOR have been described. Under nonstressed conditions, TOR phosphorylation of ABA receptors leads to inactivation of SnRK2 kinases and disrupts ABA signaling. Under abiotic stress conditions, ABA activates SnRK2 that phosphorylates RAPTOR resulting in the inhibition of TOR and consequential activation of autophagy (Wang et al., 2018).

Previous studies have shown that the main mechanism of action of sulfide involves persulfidation of reactive cysteine residues of the target proteins resulting in changes in enzyme structure, activity and subcellular localization previously demonstrated in several target plant proteins (Aroca et al., 2015; Aroca et al., 2017b; Aroca et al., 2018). A proteomic analysis performed on mature leaves from Arabidopsis plants grown under nonstress conditions revealed that a high proportion of the whole Arabidopsis proteome may undergo persulfidation under the basal conditions (Aroca et al., 2017a). In this study, a comparative and quantitative proteomic analysis has been performed on ABA-treated leaves to determine whether persulfidation mechanism is involved in sulfide regulation of the ABA signaling pathways. Significant differences in the levels of persulfidation were observed after ABA treatment compared to that under the control conditions. Surprisingly, the protein with the lowest level of persulfidation after 3 h ABA treatment was identified as Cys-type protease AtATG4a (5.20-fold change, $p<0.05$, control *versus* 3h ABA), and even after 6 h of ABA treatment, the reduction in the level of persulfidation remained very significant (2.46-fold change, $p<0.05$, control *versus* 6 h ABA). These data suggest that AtATG4a may be a target of persulfidation and that this posttranslational modification may be the molecular mechanism mediating sulfide regulation of autophagy. A detailed analysis of the ABA-triggered changes in the persulfidation proteome will be performed in a future study. Our results demonstrated that ATG4 proteolytic activity in Arabidopsis is reversibly regulated by sulfide, and this regulation effectively controls the progression of autophagy. Thus, our

findings contribute to the understanding of the mechanism of regulation of autophagy by sulfide in the plant systems and add another level of regulation to this process.

The AtATG4a protease contains a specific site of persulfidation detected by the tag-switch procedure and confirmed by mass spectrometry. The specifically persulfidated cysteine residue is Cys170, which is a part of the characteristic catalytic triad Cys-His-Asp of cysteine proteases (Sugawara et al., 2005). Comparison of the amino acid sequences of ATG4s from various biological systems indicated low similarity although the amino acids required for the cysteine protease activity, including the catalytic Cys170, are highly conserved. Interestingly, Cys170 is the only Cys residue that is conserved in all known ATG4s (Supplemental Figure 5) (Perez-Perez et al., 2014; Perez-Perez et al., 2016; Seo et al., 2016). In contrast, redox regulation of specific Cys residues has been detected in ATG4 from human, yeast, and Chlamydomonas. However, these residues are not conserved in various organisms and therefore the details of the regulatory mechanisms may be different. In humans, HsATG4a and HsATG4b proteases are the targets of reversible oxidation by H_2O_2, and the cysteine residue Cys81 located close to the catalytic Cys residue (Cys77, analogous to Cys170 in Arabidopsis) was shown to be critical for this regulation (Scherz-Shouval et al., 2007). Recently, Cys292 and Cys361 have been shown to be HsATG4b sites essential for reversible oxidative modification (Zheng et al., 2020). Redox regulation of the yeast ScATG4 protein is due to the formation of a disulfide bond between the noncatalytic residues Cys338 and Cys394, which is thioredoxin-dependent (Perez-Perez et al., 2014). In *Chlamydomonas reinhardtii*, CrATG4 activity depends on the formation of a single disulfide bond regulated by the NADPH/thioredoxin system; however, only Cys400, which is the equivalent to Cys338 in yeast, has been demonstrated to be required for redox regulation of the algal CrATG4 enzyme (Perez-Perez et al., 2016). In Arabidopsis, the activity of AtATG4a and AtATG4b is reversibly inhibited *in vitro* by reactive oxygen species (Woo et al., 2014), although redox regulation of the critical cysteine residues was not reported. Additionally, other posttranslational modifications of cysteine residues of ATG4 proteases have been described, such as S-nitrosylation of HsATG4b at Cys189 and Cys292, though these two residues are not conserved in the HsATG4a amino acid sequence (Li et al., 2017). Therefore, persulfidation of the catalytic Cys residue of cysteine proteases ATG4 can be a posttranslational modification conserved in various biological systems.

529 Because the target residue of persulfidation involves the active site, an effect of the
530 sulfide donor molecules on the enzymatic activity of AtATG4a was anticipated. In fact,
531 a 3D modelling analysis predicted that the addition of a sulfur atom to the -SH group of
532 Cys170 can cause unfavorable effects on the catalytic site of AtATG4a that should
533 affect substrate recognition and impair the enzyme activity. To test this hypothesis, a
534 heterologous activity assay was developed using CrATG8 as a substrate similar to
535 previously reported assays (Perez-Perez et al., 2014; Seo et al., 2016). Our results
536 indicate that the plant protease is functional and can process the algal substrate.
537 Our findings demonstrate that sulfide plays a specific role in the regulation of ATG4
538 enzymatic activity. The sulfide donor molecules used in this study, such as hydrosulfide
539 and tetrasulfide, significantly inactivate AtATG4a cleavage activity even at relatively
540 low concentrations, being polysulfide the most efficient inhibitor. The chemical
541 mechanism of the reaction of the thiol groups with the sulfide molecule remains a
542 matter of debate. H_2S cannot directly react directly with thiols, and the cysteine group
543 must be partially oxidized (converted to disulfide, glutathiolated, S-nitrosylated, or to
544 sulfenic acid) prior to sulfide attack. Alternatively, certain chemical studies have
545 demonstrated that sulfane sulfur (S^0) of the polysulfide molecule is responsible for the
546 production of persulfide during interaction with the thiol group (Toohey, 2011; Kimura,
547 2015; Mishanina et al., 2015). This phenomenon can explain why polysulfide is a more
548 potent inhibitor of ATG4 activity than hydrosulfide. Moreover, the inhibitory effect of
549 low concentrations of sulfide on AtATG4a activity compatible with the *in vivo*
550 conditions is reversible by a reducing agent suggesting a biological role of this effect.
551 Interestingly, an enzymatic mechanism of reversing persulfidation by the thioredoxin
552 system has been demonstrated in animal systems (Wedmann et al., 2016; Doka et al.,
553 2020). Thus, it is plausible that the thioredoxin system also functions in plants to
554 modulate the activity of AtATG4.
555 The biological significance of sulfide regulation of autophagy through reversible
556 inhibition of ATG4 protease is reinforced by the assays in Arabidopsis leaves under
557 basal and autophagy-inducing conditions. Our experimental system was shown to be
558 suitable for specific assay of Arabidopsis ATG4 processing activity by using various
559 experimental approaches. Endogenous plant ATG4 cysteine proteases specifically
560 recognize the Gly120 cleavage site in the substrate from green algae based on the
561 experiment with the G120A mutant of the CrATG8 substrate. The processed form was
562 not detected when the Arabidopsis protein extracts were deficient in ATG4a and

ATG4b enzymes, demonstrating the specificity of our experimental system. The endogenous Arabidopsis ATG4 proteins mimic the effect of sulfurating molecules on AtATG4a *in vit*ro, including significant inhibition by the sulfide donor and reversal by a reducing agent. A significant increase in the overall ATG4 protease activity in Arabidopsis was detected under autophagy-inducing conditions, including nitrogen starvation and osmotic stress. Thus, a correlation was detected between the progress of autophagy and the ATG4 enzymatic activity estimated using the heterologous assay method. Additionally, the inhibitory effect of sulfide on the protease activity was observed under the conditions of induced autophagy. Overall, our findings suggest that negative regulation of the progress of autophagy by sulfide is mediated by specific persulfidation of cysteine protease ATG4. However, additional targets of sulfide cannot be ruled out and further analysis is needed.

In conclusion, our data suggest a new level of regulation of ATG4 activity by sulfide. Based on our findings, we propose that intracellular sulfide maintains high levels of persulfidation of the ATG4 pool under basal conditions, resulting in the inhibition of ATG4 proteolytic activity. ATG4 inhibition limits the formation of ATG8-PE adducts and consequently *de novo* synthesis of autophagosomes. An increase in the intracellular level of ABA transiently reduces the level of persulfidation of the ATG4 population and then activates the protease activity of the enzyme to process ATG8 that can be further lipidated (Figure 10).

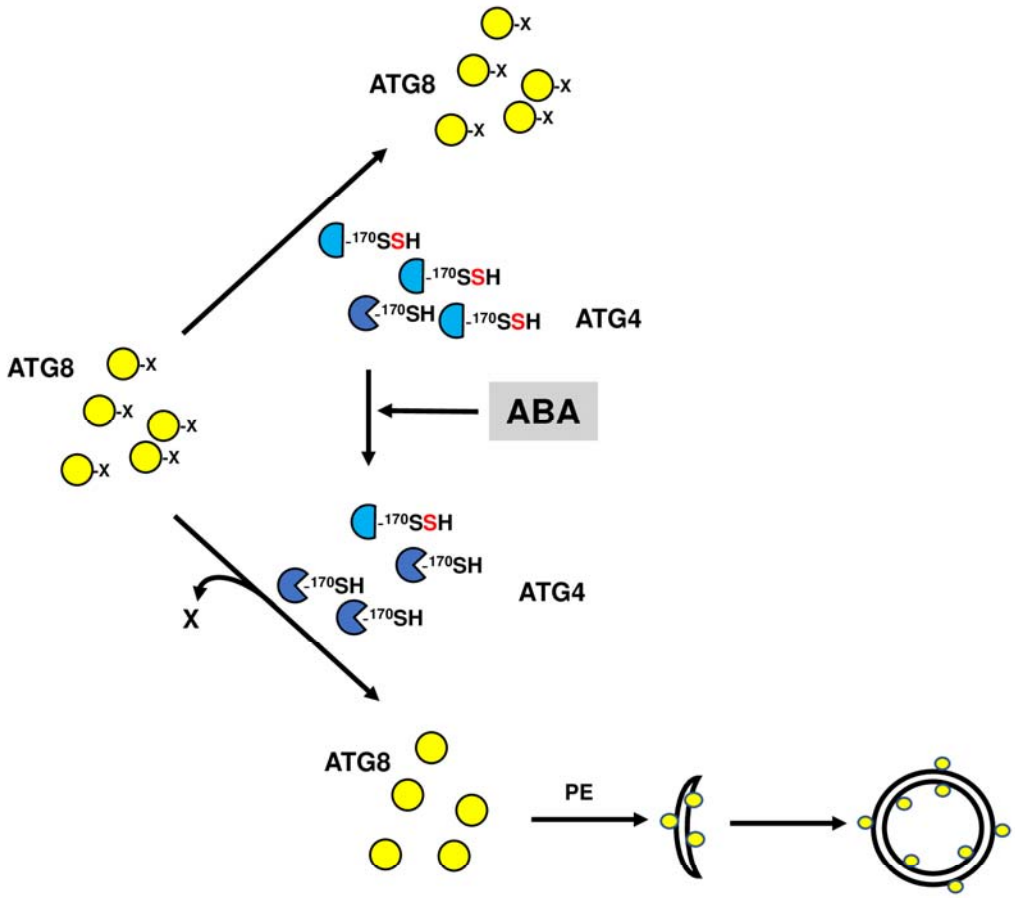

Figure 10. Graphical model of ABA-triggered autophagy induction through ATG4 posttranslational modification. Under basal conditions intracellular sulfide maintains high levels of persulfidation of the ATG4 pool which inhibits the proteolytic activity of the enzyme for ATG8 C-terminal processing. Increase in the intracellular level of ABA transiently decreases the level of persulfidation of the ATG4 population, activating the protease activity of the enzyme and the processing of ATG8 that can be further lipidated for the progression of autophagy. Yellow circles represent ATG8 protein with or without the C-terminal processed end (represented as X). Blue semicircles represent persulfidated ATG4 protein at the thiol ^{170}Cys residue. Blue Pacman symbols represent ATG4 protein with reduced thiol ^{170}Cys residue. The conjugation process of ATG8 with phosphatidylethanolamine (PE), autophagosome initiation and closure are also shown.

584

METHODS

Plant Material, Treatments and Protein Extraction

Plant growth conditions were 16 h of light (120 μE m^{-2} s^{-1}) at 22°C and 8 h of dark at 20°C. The *Arabidopsis thaliana* wild-type and the *atg4ab* mutant (Nottingham Arabidopsis Stock Center) seeds were sown on the MS solid medium containing 0.8% (w/v) agar, synchronized at 4°C for 2 d, and incubated vertically in a growth chamber. For exposure to the nitrogen-starvation conditions, nitrogen-deficient MS medium was prepared by replacing nitrate salts with chloride salts. For mannitol treatment, 300 mM was added to the MS medium. One-week-old seedlings were transferred to nitrogen-deficient or mannitol-containing MS solid medium for an additional 4 d of growth.

For proteomic analysis, wild-type Arabidopsis plants were grown in soil for 30 days, and then sprayed with water (control conditions), or 50 μM ABA for 3 and 6 h. To assess the autophagic activity, one-week-old Arabidopsis seedlings overexpressing GFP-ATG8e (Xiong et al., 2007) were transferred to the MS liquid medium and treated with 50 μM ABA for 3 and 6 h and with 200 μM NaHS for 1 h.

Arabidopsis material (200 mg) was ground in liquid nitrogen with 400 mL of extraction buffer (100 mM Tris-HCl, pH 7.5, 400 mM sucrose, 1 mM EDTA, 0.1 mM phenylmethylsulfonyl fluoride (PMSF)) using a mortar and pestle. After centrifugation at 500 *g* for 10 min at 4ºC, the supernatant was used as the Arabidopsis protein extract.

Persulfidated Protein Quantitation by Label-free SWATH-MS Acquisition and Analysis

Protein samples from three biological replicates (independent pools) of leaf tissues treated with ABA for 0 h (control sample), 3 h and 6 h were isolated and 1 mg of protein per sample was used for the tag-switch labeling for enrichment of persulfidated proteins as described (Aroca et al, 2017). After elution from the streptavidin-beads, the proteins were precipitated by TCA/acetone. Precipitated samples were resuspended in 50 mM ammonium bicarbonate with 0.2% Rapigest (Waters) for protein determination. Protein (50 μg) was digested with trypsin as described previously (García et al., 2019; Vowinckel et al., 2014), and the SWATH-MS analysis was performed at the Proteomic

618 Facility of the Institute of Plant Biochemistry and Photosynthesis, Seville, Spain. A
619 data-dependent acquisition (DDA) approach using nano-LC-MS/MS was initially
620 performed to generate the SWATH-MS spectral library as described by García et al.,
621 (2019).
622 The peptide and protein identifications was performed using Protein Pilot software
623 (version 5.0.1, Sciex) with the Paragon algorithm. The search was conducted against a
624 Uniprot proteome (June 2017, release), and the corresponding reversed entries and
625 common contaminants were assembled in the FASTA format using ProteinPilot
626 software v5.0.1 (AB Sciex) with the Paragon™ algorithm. Samples were input as
627 unlabeled with no special factors, trypsin digested and MSBT alkylated. The
628 automatically generated report in ProteinPilot™ was manually inspected for FDR (false
629 discovery rate) cut-off proteins and only proteins identified at FDR ≤1% were
630 considered for output and subsequent analysis.
631 For relative quantification using SWATH analysis, the same samples used to
632 generate the spectral library were analyzed using a data-independent acquisition (DIA)
633 method. Each sample (2 µL) was analyzed using SWATH-MS acquisition method on
634 the LC-MS equipment with the LC gradient as described. The method consisted of
635 repeated acquisition cycles of TOF MS/MS scans (230 to 1500 m/z, 60 ms acquisition
636 time) of 60 overlapping sequential precursor isolation windows of variable width (1 m/z
637 overlap) covering the 400-1250 m/z mass range from a previous TOF MS scan (400-
638 1250 m/z, 50 ms acquisition time) for each cycle. The total cycle time was 3.7 s.
639 Autocalibration of the equipment and chromatographic conditions were controlled by
640 an injection of a standard of digested β-galactosidase from *E coli* between the replicates.
641 SWATH MS spectra alignment was performed with the *PeaKView* 2.2 (*Sciex*)
642 software with the *microapp SWATH* 2.0 using the reference spectral library generated as
643 described above. Two DIA raw files for each biological replicate were loaded in unison
644 using the following parameters: 10 peptides, 7 transitions, peptide confidence >99%,
645 1% FDR including shared peptides, and XIC width set at 0.05 Da. After data
646 processing, three distinct files were exported for subsequent quantification. The
647 processed mrkvw files containing protein information from PeakView were loaded into
648 MarkerView (Version 1.2.1, AB Sciex) for normalization of protein intensity (peak
649 area) for all runs using the built-in total ion intensity sum plug-in. Log2 transformation
650 was performed prior to statistical analysis. A histogram plot was used to check the
651 normality of distribution of each technical replicate. Mean values of protein expression

were used for calculation of fold change (FC). Proteins with adjusted $p < 0.05$ and $FC \geq 1.5$ were considered differentially expressed.

The mass spectrometry proteomic data have been deposited to the ProteomeXchange Consortium via the PRIDE (Vizcaino et al, 2016) partner repository with the identifier PXD019802.

Expression of AtATG4a in *Escherichia coli*

Total RNA was extracted from wild-type Arabidopsis leaves using an RNeasy plant mini kit (Qiagen) and reverse-transcribed using an oligo (dT) primer and a SuperScript first-strand synthesis system for RT-PCR (Invitrogen). Subsequently, a 1,404 bp sequence encoding the full-length AtATG4a (At2g44140) protein was amplified by PCR using the primers ATG4-F: CACCATGAAGGCTTTATGTGA and ATG4-R: ATGACTGGCAAATGCTCTGA and the proofreading Platinum Pfx DNA polymerase (Invitrogen). The PCR conditions were as follows: a denaturation cycle of 2 min at 94°C followed by 30 amplification cycles of 15 s at 94°C, 30 s at 57°C, and 1 min at 68°C. The amplified cDNA was then ligated into the pENTR/D-TOPO vector using the pENTR directional TOPO cloning kit (Invitrogen) according to the manufacturer's instructions. Positive clones were identified by PCR and selected for plasmid DNA isolation. The *AtATG4a* cDNA was then cloned into the expression vector pDEST17 using an *E. coli* expression system with gateway technology (Invitrogen), which generates a fusion protein with an N-terminal 6x His tag that was confirmed by sequencing; the expression was induced with L-arabinose in BL21-AI *E. coli* cells.

Purification of the Recombinant AtATG4a Protein

The 6x His-tagged recombinant protein was isolated from 200 mL of BL21-AI *E. coli* cells that were cultured at 37°C to an optical density of 0.5 at 600 nm and induced with 0.2% (w/v) L-arabinose for 2.5 h at 37°C. Prior to purification, His-tagged AtATG4a was solubilized with 6 M urea because the recombinant protein was contained in the inclusion bodies. Then, the protein was purified from the soluble fraction by nickel affinity chromatography using an Invitrogen Ni-NTA Purification System (ThermoFisher Scientific), according to the manufacturer's instructions. The purified protein was concentrated and desalted using 10 kD cutoff pore size centrifugal filter

686 units (Millipore). The purity of the protein was confirmed by SDS-PAGE using 12%
687 (w/v) polyacrylamide gels stained by Coomassie Blue.
688
689 **Detection of Persulfidation on the Recombinant AtATG4a**
690
691 An untreated aliquot of the purified recombinant AtATG4a and another aliquot
692 pretreated with 50 mM DTT for 30 min at 4°C to reduce all persulfide groups were
693 precipitated with acetone for 20 min at -20°C and centrifuged at a maximum speed for
694 20 min at 4°C. After acetone removal, the proteins were resuspended in 50 mM Tris-
695 HCl (pH 8) buffer supplemented with 2.5% (w/v) SDS and subjected to the tag-switch
696 procedure as described previously (Aroca et al., 2017a). The CN-biotinylated proteins
697 were then detected using an immunoblot assay as follows. The CN-biotinylated proteins
698 were separated using nonreducing SDS-PAGE through 12% (w/v) polyacrylamide gels
699 and transferred to polyvinylidene difluoride membranes (Bio-Rad) according to the
700 manufacturer's instructions. The anti-biotin (Abcam) and secondary antibodies were
701 diluted 1:500,000 and 1:100,000, respectively, and ECL Select western blotting
702 detection reaction (GE Healthcare) was used to detect the proteins using horseradish
703 peroxidase-conjugated anti-rabbit secondary antibodies. For protein loading control, the
704 membranes before immunodetection were stained with SYPRO Ruby (Invitrogen) to
705 detect all protein bands.
706
707 **Identification of Persulfidated Cys Residues of Recombinant AtATG4a Using**
708 **Mass Spectrometry**
709
710 Recombinant AtATG4a was separated using nonreducing SDS-PAGE through 12%
711 (w/v) polyacrylamide gels, and the band corresponding to AtATG4a was manually
712 excised from Coomassie-stained gels. Gel plugs were washed twice using 50 mM
713 ammonium bicarbonate and acetonitrile and dried under a steam of nitrogen. Then,
714 proteomics-grade trypsin (Sigma-Aldrich) at a final concentration of 16 ng/µl in 25%
715 (v/v) acetonitrile/50 mM ammonium bicarbonate solution was added; the samples were
716 digested at 37ºC for 5 h. The reaction was stopped by adding 50% (v/v)
717 acetonitrile/0.5% (v/v) trifluoroacetic acid for peptide extraction. The eluted tryptic
718 peptides were dried by speed-vacuum centrifugation and resuspended in 6 µl of 0.1%

(v/v) formic acid in water. Digested peptides were subjected to nanoliquid chromatography electrospray ionization tandem mass spectrometry analysis using a nanoliquid chromatography system (ExcionLC AD, Sciex) coupled to a TripleTOF 5600+ mass spectrometer (Sciex) with a spray ionization source. Mass spectrometry and MS/MS data of individual samples were processed using the Analyst TF 1.5.1 software (Sciex). Peptide mass tolerance was set to 25 μD D^{-1} and 0.05 D for fragment masses, and only one or two missed cleavages were allowed. Peptides with an individual M_r search score $\geq$ 20 were considered correctly identified.

***In vitro* ATG4 Enzyme Activity Assay**

The typical reaction mixture contained 5 μM recombinant AtATG4a, 5 μM CrATG8 (Perez-Perez et al., 2010), and 1 mM EDTA in Tris-buffered saline (50 mM Trizma base, 138 mM NaCl, and 27 mM KCl at pH 8). When indicated, AtATG4a was incubated in the presence of DTT, TCEP, NaHS, Na_2S_4, or iodoacetamide alone or in combination at the indicated times and concentrations. The reaction mixtures were incubated at 25°C, and the reaction was stopped by the addition of β-mercaptoethanol-free Laemmli sample buffer followed by 5 min boiling. The proteins were resolved using nonreducing SDS-PAGE through 15% (w/v) polyacrylamide gels and stained with Coomassie Brilliant Blue (Sigma-Aldrich). The gels were scanned with a GS-800 densitometer (Bio-Rad), and the signals corresponding to the unprocessed and processed CrATG8 forms were quantified with the Quantity One software (Bio-Rad). The ATG4 activity (in arbitrary units) was calculated as the ratio of the band intensity of the processed CrATG8 to the sum of the intensities of the unprocessed and processed CrATG8. An activity value of 1 corresponds to the maximum value.

Assay of Endogenous ATG4 Enzyme Activity in Cell-Free Total Extract

The *in vivo* assay of ATG4 activity in cell-free total extract was performed in a typical reaction mixture containing 40 μg of leaf or 20 μg of root protein extract and 0.05 μM purified unprocessed CrATG8, processed pCrATG8, or Gly-to-Ala mutant protein (G120A). When required, a sulfur donor (Na_2S_4), a reducing agent (TCEP), or an alkylating agent (IAM) was added at the indicated concentrations. The reaction mixture

752 was incubated at 25ºC for the indicated time, stopped by addition of β-mercaptoethanol-
753 free Laemmli sample buffer, and boiled for 5 min. Then, proteins were separated using
754 nonreducing SDS-PAGE through 15% (w/v) polyacrylamide gels and transferred to
755 nitrocellulose membranes (Bio-Rad) as described previously (Perez-Perez et al., 2010).
756 Anti-CrATG8 (Pérez-Pérez et al., 2010) and secondary antibodies were diluted 1:3,000
757 and 1:10,000, respectively. An ECL Select western blotting detection reaction (GE
758 Healthcare) was used to detect the proteins. For protein loading control, the membranes
759 before immunodetection were stained with Ponceau S (Sigma-Aldrich) to detect all
760 protein bands.
761
762 **Protein modeling**
763
764 3D homology modeling was driven by Modeller (Sali and Blundell, 1993) using the
765 structure of the *Homo sapiens* Atg4B-LC3 complex (PDB ID: 2Z0E) (Sato et al., 2009)
766 as a template. Molecular crystal X-ray structures and structural model of *Arabidopsis*
767 *thaliana* AtATG4a-AtATG8a complex were inspected, analyzed and plotted with
768 PyMol 1.4.1 (Schrodinger LLC). Surface electrostatic potentials were calculated and
769 visualized using the PyMol 1.4.1 sofware.
770
771
772 **Accession Numbers**
773
774 The mass spectrometry proteomic data have been deposited to the ProteomeXchange
775 Consortium via the PRIDE partner repository with the identifier PXD019802. Sequence
776 data from this article can be found in the EMBL/GenBank data libraries under the
777 following accession numbers: *AtATG4a* (At2g44140), *AtATG4b* (At3g59950), *AtATG8a*
778 (At4g21980) and *CrATG8* (Cre16.g689650.t1.1).
779
780
781
782 **Supplemental Data**
783
784 **Supplemental Dataset 1.** Spectral library
785

Supplemental Dataset 2. Proteins quantified using SWATH acquisition method in the control sample versus 3 h ABA treatment sample.

Supplemental Dataset 3. Proteins with different abundance in the control sample compared to that in the 3 h ABA treatment sample at p value <0.05.

Supplemental Dataset 4. Proteins quantified using SWATH acquisition method in the control sample versus 6 h ABA treatment sample.

Supplemental Dataset 5. Proteins with different abundance in the control sample compared to that in the 6 h ABA treatment sample at p value <0.05.

Supplemental Table 1. Classification of the proteins with persulfidation level reduced after 3 h ABA treatment.

Supplemental Table 2. Protein list of the elements included in the bin of "proteins" with persulfidation level reduced after 3 h ABA treatment.

Supplemental Figure 1. C-Terminus of nine Arabidopsis and the Chlamydomonas ATG8 proteins.

Supplemental Figure 2. Simulation of surface electrostatic potential distribution in the HsATG4b-LC3 protein complex (PDB ID: 2Z0E) and AtATG4a-AtATG8a 3D structural model.

Supplemental Figure 3. Conjugation of Chlamydomonas ATG8 processed by ATG4s proteases from Arabidopsis.

Supplemental Figure 4. Phenotypes of wild-type and *atg4ab* double-mutant seedlings under the basal and induced autophagy conditions.

Supplemental Figure 5. Alignment of amino acid sequences of ATG4 from various sources.

Supplemental Figure 6. Lower exposition of the GFP-blot shown in Figure 2.

ACKNOWLEDGMENTS

This work was supported in part by the European Regional Development Fund through the Ministerio de Economía y Competitividad and the Agencia Estatal de Investigación grants BFU2015-68216-P and PGC2018-099048-B-I00 (to J.L.C.); grants BIO2015-74432-JIN and PID2019-110080GB-I00 (to M.E.P-P.); grants BIO2016-76633-P and PID2019-109785GB-I00, and Junta de Andalucía grant P18-RT-3154 (to C.G.)., the Marie Skłodowska-Curie grant agreement No. 834120 (to A.A.), and Government of Aragón-FEDER grant E35_17R (to I. Y.). A.M. L-M. and A. J-F. were supported by the Ministerio de Economia y Competitividad through the program of "Formación de Personal Investigador". We want to thank Dr. Rocío Rodríguez for the Proteomics Services.

AUTHOR CONTRIBUTIONS

Á.A., A.M.L-M., M.E.P-P., I.Y., A. J-F. and I.M. performed research and analyzed the data. J.L.C. and L.C.R. designed research and analyze data. C.G. designed the research, analyzed the data, and wrote the article. All authors contributed to the discussion.

Figure Legends

Figure 1. Proteomic analysis of protein persulfidation in response to ABA in mesophyll cells.

(A) Workflow of ABA leaf treatments followed by tag-switch protein labeling with CN-biotin, protein purification, and quantitative SWATH analysis of eluted proteins.

(B) PCA representation plot of the 18 samples after SWATH analysis. Score for PC1 (70 %) versus PC2 (9.9%), Pareto scaling.

(C) Level of persulfidated ATG4a after ABA treatments. Values represent the mean peak areas of extracted ion chromatogram of identified ATG4a peptides. *, $p < 0.05$.

Figure 2. Effect of sulfide on autophagy induced by ABA treatment.

(A) Immunoblot analysis of GFP-ATG8e fusion protein. One-week-old seedlings expressing GFP-ATG8e fusion protein were transferred to liquid MS media and were not treated (control) or treated with 50 μM ABA for 3 and 6 h and then 200 μM NaHS for 1 h. Total protein extracts were prepared and subjected to SDS-PAGE and immunoblot analysis with anti-GFP antibodies. Anti-tubulin antibodies were used as the protein-loading control.

(B) Quantification of the free GFP/GFP-ATG8 ratio. For each condition, the levels of free GFP and GFP-ATG8e fusion protein were quantified in a less exposed blot shown in Supplemental Figure 6. The value of 100% was assigned to the free GFP/GFP-ATG8 ratio of the control sample. Data are from three independent experiments and evaluated by two-factor ANOVA. Same letters indicate no significant differences. $P < 0.05$.

Figure 3. Persulfidation of Arabidopsis AtATG4a.

(A) Immunoblot analysis of persulfidated AtATG4a. Purified recombinant AtATG4a was treated in the absence (-) or in the presence of 50 mM DTT (+) for 30 min at 4ºC, dialyzed, and subjected to the tag-switch labeling as described in the Methods. Then, the proteins were subjected to immunoblot analysis using anti-biotin antibodies. Sypro Ruby fluorescent staining is shown as the protein loading control.

(B) Analysis of AtATG4a using mass spectrometry. LC-MS/MS analysis of a tryptic peptide of AtATG4a containing Cys170. The table inside the spectrum contains the predicted ion types for the modified peptide, and the ions detected in the spectrum are highlighted in red.

(C) AtATG4a protein sequence identified with 97% coverage. The peptide containing persulfidated Cys170 is highlighted in yellow and all the Cys residues are red.

Figure 4. Arabidopsis ATG4a cleaves Chlamydomonas ATG8.

ATG4 activity of the recombinant AtATG4a was assayed by monitoring the cleavage of CrATG8 from the unprocessed (CrATG8) to processed (pCrATG8) forms (indicated by arrowheads) using SDS-PAGE followed by Coomassie Blue staining and quantification of protein band intensities. The ATG4 activity (relative units) was determined as the ratio of the band intensity of the processed CrATG8 to the sum of the intensities of the unprocessed and processed CrATG8. Activity value of 1 corresponds to the maximum. Processed pCrATG8 (lane 1) and unprocessed CrATG8 (lane 2) were loaded as controls. Representative images are shown. Data are from three independent experiments and evaluated by two-factor ANOVA. Same letters indicate no significant differences. $P < 0.05$.

(A) Effect of incubation time. AtATG4a was incubated with CrATG8 in the absence or in the presence of 10 mM DTT for the indicated times.

(B) Effect of DTT concentration. AtATG4a was incubated with CrATG8 in the absence or in the presence of increasing concentrations of DTT for 4 h.

(C) Effect of TCEP concentration. AtATG4a was incubated with CrATG8 in the absence or in the presence of increasing concentrations of TCEP for 4 h.

Figure 5. Effect of NaHS on AtATG4a enzyme activity.

(A) AtATG4a was incubated with 0.5 mM TCEP for 2 h and treated in the absence or in the presence of indicated concentrations of NaHS for 1 h. Then, CrATG8 was added to the incubation mixture, and ATG4 activity was monitored after 4 h using Coomassie-stained gels as described in the Methods. All procedures were performed at 25ºC. Lane 1 and 2, unprocessed and processed CrATG8, respectively. Lane 3, AtATG4a incubated with CrATG8 in the absence of TCEP and of NaHS. Lanes 4-8, TCEP-pretreated reduced AtATG4a incubated with CrATG8 in the presence of increasing concentrations of NaHS (from 0 to 1 mM). A representative image is shown.

(B) Quantification of ATG4 activity (relative units) determined as the ratio of the band intensity of the processed CrATG8 to the sum of the intensities of the unprocessed and processed CrATG8. A value of 1 corresponds to AtATG4a in the absence of NaHS (lane 4).

(C) Quantification of the protein band intensity corresponding to the monomeric AtATG4a form marked by a rectangle in A. A value of 100% corresponds to AtATG4a in the absence of NaHS (lane 4).
Data are from three independent experiments and evaluated by two-factor ANOVA. Same letters indicate no significant differences. $P < 0.05$.

Figure 6. Effect of polysulfides on AtATG4a enzyme activity.
(A) AtATG4a was incubated with 0.5 mM TCEP for 2 h and subsequently treated in the absence or in the presence of indicated concentrations of Na_2S_4 for 1 h. Then, CrATG8 was added to the incubation mixture, and ATG4 activity was monitored after 4 h using Coomassie-stained gels as described in Methods. All procedures were performed at 25 ºC. A representative image is shown.
(B) Quantification of ATG4 activity (relative units) determined as the ratio of the band intensity of the processed CrATG8 to the sum of the intensities of the unprocessed and processed CrATG8. A value of 1 corresponds to AtATG4a treated in the absence of Na_2S_4 (lane 1).
(C) Quantification of the protein band intensity corresponding to the monomeric AtATG4a form marked by a rectangle in A. A value of 100% corresponds to AtATG4a treated in the absence of Na_2S_4 (lane 1).
(D) Reversibility of the effect. AtATG4a was incubated with 0.25 mM TCEP for 2 h (lane 1) and treated with 100 µM Na_2S_4 for 1 h (lane 2) and 1 mM TCEP for 1 h (lane 3). ATG4 activity was monitored using Coomassie-stained gels. The experiment was performed at least three times and a representative image used for the quantification of the activity is shown.
Data are from three independent experiments and evaluated by two-factor ANOVA. Same letters indicate no significant differences. $P < 0.05$.

Figure 7. Predicted structure of the AtATG4a-AtATG8a complex.
(A) 3D modelling of the AtATG4a-AtATG8a complex based on the structure of the HsAtg4B-LC3 protein complex (PDB ID: 2Z0E). The AtATG8 protein sequence (Q8LEM4 in UniProtkB) corresponds to the splice variant 1. Surface representation of the protein complex and the equivalent residues surrounding the catalytic cavity

Cys170, Trp192, Asp364, and His366 in AtATG4a (red) and Phe116, Gly117, Thr120, and Ala122 in AtATG8a (blue) are shown in the structural models.
(B) Zoomed view of the putative conformation of the active site showing the spheres corresponding to the position and distance (Å) of catalytic residues Cys170, Trp192, Asp364, and His366 in AtATG4a.

Figure 8. Cleavage and conjugation of Chlamydomonas ATG8 by Arabidopsis proteins.
(A) ATG4 proteolytic activity in wild-type Arabidopsis leaves. Arabidopsis protein extracts prepared from leaves of wild-type seedlings grown for 11 days on MS medium were incubated with CrATG8 or site-directed mutant G120A proteins at 25ºC for the indicated times, and ATG4 activity was monitored as the cleavage of the ATG8 forms to the processed (pCrATG8) forms by immunoblotting analysis with anti-CrATG8. Processed pCrATG8 (lane 1), unprocessed CrATG8 (lane 2), and site-directed mutant G120A (lane 6) were loaded as controls.
(B) ATG4 proteolytic activity in the Arabidopsis *atg4ab* mutant. Arabidopsis protein extracts were prepared from the leaves of wild-type and *atg4ab* double mutant seedlings grown for 7 days on the MS medium and transferred to the same medium (+N) or to a nitrogen-deficient medium (-N) for additional 4 days. The protein extracts were incubated with CrATG8 at 25ºC, and ATG4 activity was monitored after 0, 0.5, or 2 h as indicated by immunoblotting analysis with anti-CrATG8.
The arrowheads show the unprocessed CrATG8 and processed pCrATG8 protein bands, and the asterisks indicate faster-mobility protein bands. Ponceau staining is shown as the protein loading control of the Arabidopsis extract.

Figure 9. Sulfide inhibits the endogenous proteolytic activity of Arabidopsis ATG4.
(A) Effect of polysulfides on endogenous enzyme activity of Arabidopsis ATG4. Arabidopsis protein extracts (Ex) were prepared from the leaves of seedlings grown for 11 days on the MS medium. The extracts were treated in the absence (un-Ex) and in the presence of 200 μM Na_2S_4 (Na_2S_4-Ex), or 20 mM iodoacetamide (IAM-Ex) for 30 min, or in the presence of 200 μM Na_2S_4 for 30 min and 1 mM TCEP for 30 min (Na_2S_4-Ex + TCEP). Then, CrATG8 was added to the incubation mixture, and ATG4 proteolytic activity was monitored. Lane 1, unprocessed CrATG8.

(B) Sulfide reverts the endogenous enzyme activity of Arabidopsis ATG4 under autophagy-induced conditions. Arabidopsis protein extracts were prepared from the leaves of seedlings grown for 7 days on the MS medium and transferred to the same medium (+N) or to a nitrogen-deficient medium (-N) (left panel); or transferred to the same medium (-mannitol) or to same medium containing 300 mM mannitol (+mannitol) (right panel) for additional 4 days. The extracts were treated in the absence (un-Ex) or in the presence of 200 μM Na_2S_4 for 30 min (Na_2S_4-EX); CrATG8 was added to the incubation mixture and ATG4 activity was monitored. Lane 1, processed pCrATG8 and lane 2, unprocessed CrATG8.

The ATG4 activity was monitored at the indicated times by immunoblotting analysis with anti-CrATG8. All procedures were performed at 25ºC. Ponceau staining is shown as the protein loading control.

Figure 10. Graphical model of ABA-triggered induction of autophagy mediated by posttranslational modification of ATG4. Under basal conditions, intracellular sulfide maintains high levels of persulfidation of the ATG4 pool, which inhibits the proteolytic activity of the enzyme for ATG8 C-terminal processing. An increase in the intracellular level of ABA transiently decreases the level of persulfidation of the ATG4 population activating the protease activity of the enzyme and the processing of ATG8 that can be further lipidated to progress autophagy. Yellow circles represent ATG8 protein with or without the processed C-terminus (represented as X). Blue semicircles represent persulfidated ATG4 at the thiol group of Cys170 residue. Blue Pacman symbols represent ATG4 with reduced thiol group of Cys170 residue. The conjugation process of ATG8 with phosphatidylethanolamine (PE) and autophagosome initiation and closure are also shown.

Parsed Citations

Alvarez C, Garcia I, Moreno I, Perez-Perez ME, Crespo JL, Romero LC, Gotor C (2012) Cysteine-generated sulfide in the cytosol negatively regulates autophagy and modulates the transcriptional profile in Arabidopsis. Plant Cell 24: 4621-4634.
Google Scholar: Author Only Title Only Author and Title

Aroca A, Gotor C, Romero LC (2018) Hydrogen Sulfide Signaling in Plants: Emerging Roles of Protein Persulfidation. Front Plant Sci 9.
Google Scholar: Author Only Title Only Author and Title

Aroca A, Benito JM, Gotor C, Romero LC (2017a) Persulfidation proteome reveals the regulation of protein function by hydrogen sulfide in diverse biological processes in Arabidopsis. J Exp Bot 68: 4915-4927.
Google Scholar: Author Only Title Only Author and Title

Aroca A, Schneider M, Scheibe R, Gotor C, Romero LC (2017b) Hydrogen Sulfide Regulates the Cytosolic/Nuclear Partitioning of Glyceraldehyde-3-Phosphate Dehydrogenase by Enhancing its Nuclear Localization. Plant Cell Physiol 58: 983-992.
Google Scholar: Author Only Title Only Author and Title

Aroca Á, Serna A, Gotor C, Romero LC (2015) S-Sulfhydration: A Cysteine Posttranslational Modification in Plant Systems. Plant Physiol 168: 334-342.
Google Scholar: Author Only Title Only Author and Title

Calderwood A, Kopriva S (2014) Hydrogen sulfide in plants: From dissipation of excess sulfur to signaling molecule. Nitric Oxide 41C: 72-78.
Google Scholar: Author Only Title Only Author and Title

Chen S, Jia H, Wang X, Shi C, Wang X, Ma P, Wang J, Ren M, Li J (2020) Hydrogen Sulfide Positively Regulates Abscisic Acid Signaling through Persulfidation of SnRK2.6 in Guard Cells. Mol Plant.
Google Scholar: Author Only Title Only Author and Title

Chung T, Phillips AR, Vierstra RD (2010) ATG8 lipidation and ATG8-mediated autophagy in Arabidopsis require ATG12 expressed from the differentially controlled ATG12A AND ATG12B loci. Plant J 62: 483-493.
Google Scholar: Author Only Title Only Author and Title

Doelling JH, Walker JM, Friedman EM, Thompson AR, Vierstra RD (2002) The APG8/12-activating enzyme APG7 is required for proper nutrient recycling and senescence in Arabidopsis thaliana. J Biol Chem 277: 33105-33114.
Google Scholar: Author Only Title Only Author and Title

Doka E, Ida T, Dagnell M, Abiko Y, Luong NC, Balog N, Takata T, Espinosa B, Nishimura A, Cheng Q, Funato Y, Miki H, Fukuto JM, Prigge JR, Schmidt EE, Arner ESJ, Kumagai Y, Akaike T, Nagy P (2020) Control of protein function through oxidation and reduction of persulfidated states. Sci Adv 6: eaax8358.
Google Scholar: Author Only Title Only Author and Title

Dong Y, Silbermann M, Speiser A, Forieri I, Linster E, Poschet G, Allboje Samami A, Wanatabe M, Sticht C, Teleman AA, Deragon JM, Saito K, Hell R, Wirtz M (2017) Sulfur availability regulates plant growth via glucose-TOR signaling. Nat Commun 8: 1174.
Google Scholar: Author Only Title Only Author and Title

Garcia-Mata C, Lamattina L (2013) Gasotransmitters are emerging as new guard cell signaling molecules and regulators of leaf gas exchange. Plant Sci 201-202: 66-73.
Google Scholar: Author Only Title Only Author and Title

Gotor C, Garcia I, Crespo JL, Romero LC (2013) Sulfide as a signaling molecule in autophagy. Autophagy 9: 609-611.
Google Scholar: Author Only Title Only Author and Title

Gotor C, Laureano-Marin AM, Moreno I, Aroca A, Garcia I, Romero LC (2015) Signaling in the plant cytosol: cysteine or sulfide? Amino Acids 47: 2155-2164.
Google Scholar: Author Only Title Only Author and Title

Gotor C, Laureano-Marín AM, Arenas-Alfonseca L, Moreno I, Aroca Á, García I, Romero LC. (2017). Advances in Plant Sulfur Metabolism and Signaling. In Progress in Botany Vol. 78, F.M. Cánovas, U. Lüttge, and R. Matyssek, eds (Cham: Springer International Publishing), pp. 45-66.
Google Scholar: Author Only Title Only Author and Title

Gotor C, Garcia I, Aroca A, Laureano-Marin AM, Arenas-Alfonseca L, Jurado-Flores A, Moreno I, Romero LC (2019) Signaling by hydrogen sulfide and cyanide through posttranslational modification. J Exp Bot.
Google Scholar: Author Only Title Only Author and Title

Gu L, Jung HJ, Kim BM, Xu T, Lee K, Kim YO, Kang H (2015) A chloroplast-localized S1 domain-containing protein SRRP1 plays a role in Arabidopsis seedling growth in the presence of ABA. J Plant Physiol 189: 34-41.
Google Scholar: Author Only Title Only Author and Title

Guiboileau A, Avila-Ospina L, Yoshimoto K, Soulay F, Azzopardi M, Marmagne A, Lothier J, Masclaux-Daubresse C (2013) Physiological and metabolic consequences of autophagy deficiency for the management of nitrogen and protein resources in Arabidopsis leaves depending on nitrate availability. New Phytol 199: 683-694.

Google Scholar: Author Only Title Only Author and Title

Hanaoka H, Noda T, Shirano Y, Kato T, Hayashi H, Shibata D, Tabata S, Ohsumi Y (2002) Leaf senescence and starvation-induced chlorosis are accelerated by the disruption of an Arabidopsis autophagy gene. Plant Physiol 129: 1181-1193.
Google Scholar: Author Only Title Only Author and Title

Ida T, Sawa T, Ihara H, Tsuchiya Y, Watanabe Y, Kumagai Y, Suematsu M, Motohashi H, Fujii S, Matsunaga T, Yamamoto M, Ono K, Devarie-Baez NO, Xian M, Fukuto JM, Akaike T (2014) Reactive cysteine persulfides and S-polythiolation regulate oxidative stress and redox signaling. Proc Natl Acad Sci USA 111: 7606-7611.
Google Scholar: Author Only Title Only Author and Title

Jin Z, Pei Y (2015) Physiological Implications of Hydrogen Sulfide in Plants: Pleasant Exploration behind Its Unpleasant Odour. Oxid Med Cell Longev 2015: 397502.
Google Scholar: Author Only Title Only Author and Title

Jin Z, Xue S, Luo Y, Tian B, Fang H, Li H, Pei Y (2013) Hydrogen sulfide interacting with abscisic acid in stomatal regulation responses to drought stress in Arabidopsis. Plant Physiol Biochem 62: 41-46.
Google Scholar: Author Only Title Only Author and Title

Kimura H (2015) Hydrogen sulfide and polysulfides as signaling molecules. Proc Jpn Acad Ser B Phys Biol Sci 91: 131-159.
Google Scholar: Author Only Title Only Author and Title

Kirisako T, Ichimura Y, Okada H, Kabeya Y, Mizushima N, Yoshimori T, Ohsumi M, Takao T, Noda T, Ohsumi Y (2000) The reversible modification regulates the membrane-binding state of Apg8/Aut7 essential for autophagy and the cytoplasm to vacuole targeting pathway. J Cell Biol 151: 263-276.
Google Scholar: Author Only Title Only Author and Title

Klie S, Nikoloski Z (2012) The Choice between MapMan and Gene Ontology for Automated Gene Function Prediction in Plant Science. Front Genet 3: 115.
Google Scholar: Author Only Title Only Author and Title

Laureano-Marin AM, Moreno I, Romero LC, Gotor C (2016a) Negative Regulation of Autophagy by Sulfide Is Independent of Reactive Oxygen Species. Plant Physiol 171: 1378-1391.
Google Scholar: Author Only Title Only Author and Title

Laureano-Marin AM, Moreno I, Aroca Á, García I, Romero LC, Gotor C. (2016b). Regulation of Autophagy by Hydrogen Sulfide. In Gasotransmitters in Plants: The Rise of a New Paradigm in Cell Signaling, L. Lamattina and C. García-Mata, eds (Cham: Springer International Publishing), pp. 53-75.
Google Scholar: Author Only Title Only Author and Title

Li Y, Zhang Y, Wang L, Wang P, Xue Y, Li X, Qiao X, Zhang X, Xu T, Liu G, Li P, Chen C (2017) Autophagy impairment mediated by S-nitrosation of ATG4B leads to neurotoxicity in response to hyperglycemia. Autophagy 13: 1145-1160.
Google Scholar: Author Only Title Only Author and Title

Liu Y, Bassham DC (2012) Autophagy: pathways for self-eating in plant cells. Annu Rev Plant Biol 63: 215-237.
Google Scholar: Author Only Title Only Author and Title

Liu Y, Xiong Y, Bassham DC (2009) Autophagy is required for tolerance of drought and salt stress in plants. Autophagy 5: 954-963.
Google Scholar: Author Only Title Only Author and Title

Marshall RS, Vierstra RD (2018a) Autophagy: The Master of Bulk and Selective Recycling. Annu Rev Plant Biol.
Google Scholar: Author Only Title Only Author and Title

Marshall RS, Vierstra RD (2018b) Autophagy: The Master of Bulk and Selective Recycling. Annu Rev Plant Biol 69: 173-208.
Google Scholar: Author Only Title Only Author and Title

Masclaux-Daubresse C, Chen Q, Have M (2017) Regulation of nutrient recycling via autophagy. Curr Opin Plant Biol 39: 8-17.
Google Scholar: Author Only Title Only Author and Title

Mishanina TV, Libiad M, Banerjee R (2015) Biogenesis of reactive sulfur species for signaling by hydrogen sulfide oxidation pathways. Nat Chem Biol 11: 457-464.
Google Scholar: Author Only Title Only Author and Title

Mizushima N, Yoshimori T, Ohsumi Y (2011) The role of Atg proteins in autophagosome formation. Annu Rev Cell Dev Biol 27: 107-132.
Google Scholar: Author Only Title Only Author and Title

Mustafa AK, Gadalla MM, Sen N, Kim S, Mu W, Gazi SK, Barrow RK, Yang G, Wang R, Snyder SH (2009) H2S signals through protein S-sulfhydration. Sci Signal 2: ra72.
Google Scholar: Author Only Title Only Author and Title

Nair U, Yen W-L, Mari M, Cao Y, Xie Z, Baba M, Reggiori F, Klionsky DJ (2012) A role for Atg8–PE deconjugation in autophagosome biogenesis. Autophagy 8: 780-793.
Google Scholar: Author Only Title Only Author and Title

Nakatogawa H, Ishii J, Asai E, Ohsumi Y (2012) Atg4 recycles inappropriately lipidated Atg8 to promote autophagosome biogenesis. Autophagy 8: 177-186.
Google Scholar: Author Only Title Only Author and Title

Papanatsiou M, Scuffi D, Blatt MR, García-Mata C (2015) Hydrogen Sulfide Regulates Inward-Rectifying K+ Channels in Conjunction with Stomatal Closure. Plant Physiol 168: 29-35.
Google Scholar: Author Only Title Only Author and Title

Paul BD, Snyder SH (2012) H2S signalling through protein sulfhydration and beyond. Nat Rev Mol Cell Biol 13: 499-507.
Google Scholar: Author Only Title Only Author and Title

Perez-Perez ME, Florencio FJ, Crespo JL (2010) Inhibition of Target of Rapamycin Signaling and Stress Activate Autophagy in Chlamydomonas reinhardtii. Plant Physiol 152: 1874-1888.
Google Scholar: Author Only Title Only Author and Title

Perez-Perez ME, Lemaire SD, Crespo JL (2016) Control of Autophagy in Chlamydomonas Is Mediated through Redox-Dependent Inactivation of the ATG4 Protease. Plant Physiol 172: 2219-2234.
Google Scholar: Author Only Title Only Author and Title

Perez-Perez ME, Zaffagnini M, Marchand CH, Crespo JL, Lemaire SD (2014) The yeast autophagy protease Atg4 is regulated by thioredoxin. Autophagy 10: 1953-1964.
Google Scholar: Author Only Title Only Author and Title

Pérez-Pérez ME, Lemaire SD, Crespo JL (2012) Reactive oxygen species and autophagy in plants and algae. Plant Physiol 160: 156-164.
Google Scholar: Author Only Title Only Author and Title

Phillips AR, Suttangkakul A, Vierstra RD (2008) The ATG12-conjugating enzyme ATG10 Is essential for autophagic vesicle formation in Arabidopsis thaliana. Genetics 178: 1339-1353.
Google Scholar: Author Only Title Only Author and Title

Romero LC, Garcia I, Gotor C (2013) L-Cysteine Desulfhydrase 1 modulates the generation of the signaling molecule sulfide in plant cytosol. Plant Signal Behav 8: e24007.
Google Scholar: Author Only Title Only Author and Title

Sali A, Blundell TL (1993) Comparative protein modelling by satisfaction of spatial restraints. J Mol Biol 234: 779-815.
Google Scholar: Author Only Title Only Author and Title

Sato A, Sato Y, Fukao Y, Fujiwara M, Umezawa T, Shinozaki K, Hibi T, Taniguchi M, Miyake H, Goto DB, Uozumi N (2009) Threonine at position 306 of the KAT1 potassium channel is essential for channel activity and is a target site for ABA-activated SnRK2/OST1/SnRK2.6 protein kinase. Biochem J 424: 439-448.
Google Scholar: Author Only Title Only Author and Title

Satoo K, Noda NN, Kumeta H, Fujioka Y, Mizushima N, Ohsumi Y, Inagaki F (2009) The structure of Atg4B-LC3 complex reveals the mechanism of LC3 processing and delipidation during autophagy. EMBO J 28: 1341-1350.
Google Scholar: Author Only Title Only Author and Title

Scherz-Shouval R, Shvets E, Fass E, Shorer H, Gil L, Elazar Z (2007) Reactive oxygen species are essential for autophagy and specifically regulate the activity of Atg4. EMBO J 26: 1749-1760.
Google Scholar: Author Only Title Only Author and Title

Scuffi D, Álvarez C, Laspina N, Gotor C, Lamattina L, García-Mata C (2014) Hydrogen Sulfide Generated by l-Cysteine Desulfhydrase Acts Upstream of Nitric Oxide to Modulate Abscisic Acid-Dependent Stomatal Closure. Plant Physiol 166: 2065-2076.
Google Scholar: Author Only Title Only Author and Title

Scuffi D, Nietzel T, Di Fino LM, Meyer AJ, Lamattina L, Schwarzländer M, Laxalt AM, García-Mata C (2018) Hydrogen Sulfide Increases Production of NADPH Oxidase-Dependent Hydrogen Peroxide and Phospholipase D-Derived Phosphatidic Acid in Guard Cell Signaling. Plant Physiol 176: 2532.
Google Scholar: Author Only Title Only Author and Title

Sen N (2017) Functional and Molecular Insights of Hydrogen Sulfide Signaling and Protein Sulfhydration. J Mol Biol 429: 543-561.
Google Scholar: Author Only Title Only Author and Title

Seo E, Woo J, Park E, Bertolani SJ, Siegel JB, Choi D, Dinesh-Kumar SP (2016) Comparative analyses of ubiquitin-like ATG8 and cysteine protease ATG4 autophagy genes in the plant lineage and cross-kingdom processing of ATG8 by ATG4. Autophagy 12: 2054-2068.
Google Scholar: Author Only Title Only Author and Title

Shen J, Zhang J, Zhou M, Zhou H, Cui B, Gotor C, Romero LC, Fu L, Yang J, Foyer CH, Pan Q, Shen W, Xie Y (2020) Persulfidation-based Modification of Cysteine Desulfhydrase and the NADPH Oxidase RBOHD Controls Guard Cell Abscisic Acid Signaling. Plant Cell 32: 1000-1017.
Google Scholar: Author Only Title Only Author and Title

Shu CW, Drag M, Bekes M, Zhai D, Salvesen GS, Reed JC (2010) Synthetic substrates for measuring activity of autophagy proteases:

autophagins (Atg4). Autophagy 6: 936-947.
Google Scholar: Author Only Title Only Author and Title

Soto-Burgos J, Zhuang X, Jiang L, Bassham DC (2018) Dynamics of Autophagosome Formation. Plant Physiol 176: 219-229.
Google Scholar: Author Only Title Only Author and Title

Sugawara K, Suzuki NN, Fujioka Y, Mizushima N, Ohsumi Y, Inagaki F (2005) Structural basis for the specificity and catalysis of human Atg4B responsible for mammalian autophagy. J Biol Chem 280: 40058-40065.
Google Scholar: Author Only Title Only Author and Title

Thimm O, Blasing O, Gibon Y, Nagel A, Meyer S, Kruger P, Selbig J, Muller LA, Rhee SY, Stitt M (2004) MAPMAN: a user-driven tool to display genomics data sets onto diagrams of metabolic pathways and other biological processes. Plant J 37: 914-939.
Google Scholar: Author Only Title Only Author and Title

Toohey JI (2011) Sulfur signaling: is the agent sulfide or sulfane? Anal Biochem 413: 1-7.
Google Scholar: Author Only Title Only Author and Title

Ustun S, Hafren A, Hofius D (2017) Autophagy as a mediator of life and death in plants. Curr Opin Plant Biol 40: 122-130.
Google Scholar: Author Only Title Only Author and Title

Vanhee C, Batoko H (2011) Autophagy involvement in responses to abscisic acid by plant cells. Autophagy 7: 655-656.
Google Scholar: Author Only Title Only Author and Title

Vanhee C, Zapotoczny G, Masquelier D, Ghislain M, Batoko H (2011) The Arabidopsis Multistress Regulator TSPO Is a Heme Binding Membrane Protein and a Potential Scavenger of Porphyrins via an Autophagy-Dependent Degradation Mechanism. The Plant Cell 23: 785-805.
Google Scholar: Author Only Title Only Author and Title

Vitvitsky V, Miljkovic JL, Bostelaar T, Adhikari B, Yadav PK, Steiger AK, Torregrossa R, Pluth MD, Whiteman M, Banerjee R, Filipovic MR (2018) Cytochrome c Reduction by H2S Potentiates Sulfide Signaling. ACS Chem Biol 13: 2300-2307.
Google Scholar: Author Only Title Only Author and Title

Wang M, Tang W, Zhu YZ (2017) An Update on AMPK in Hydrogen Sulfide Pharmacology. Front Pharmacol 8: 810.
Google Scholar: Author Only Title Only Author and Title

Wang P, Zhao Y, Li Z, Hsu CC, Liu X, Fu L, Hou YJ, Du Y, Xie S, Zhang C, Gao J, Cao M, Huang X, Zhu Y, Tang K, Wang X, Tao WA, Xiong Y, Zhu JK (2018) Reciprocal Regulation of the TOR Kinase and ABA Receptor Balances Plant Growth and Stress Response. Mol Cell 69: 100-112 e106.
Google Scholar: Author Only Title Only Author and Title

Wedmann R, Onderka C, Wei S, Szijarto IA, Miljkovic JL, Mitrovic A, Lange M, Savitsky S, Yadav PK, Torregrossa R, Harrer EG, Harrer T, Ishii I, Gollasch M, Wood ME, Galardon E, Xian M, Whiteman M, Banerjee R, Filipovic MR (2016) Improved tag-switch method reveals that thioredoxin acts as depersulfidase and controls the intracellular levels of protein persulfidation. Chem Sci 7: 3414-3426.
Google Scholar: Author Only Title Only Author and Title

Woo J, Park E, Dinesh-Kumar SP (2014) Differential processing of Arabidopsis ubiquitin-like Atg8 autophagy proteins by Atg4 cysteine proteases. Proc Natl Acad Sci U S A 111: 863-868.
Google Scholar: Author Only Title Only Author and Title

Wu D, Wang H, Teng T, Duan S, Ji A, Li Y (2018) Hydrogen sulfide and autophagy: A double edged sword. Pharmacol Res 131: 120-127.
Google Scholar: Author Only Title Only Author and Title

Xiong Y, Contento AL, Bassham DC (2005) AtATG18a is required for the formation of autophagosomes during nutrient stress and senescence in Arabidopsis thaliana. Plant J 42: 535-546.
Google Scholar: Author Only Title Only Author and Title

Xiong Y, Contento AL, Nguyen PQ, Bassham DC (2007) Degradation of oxidized proteins by autophagy during oxidative stress in Arabidopsis. Plant Physiol 143: 291-299.
Google Scholar: Author Only Title Only Author and Title

Yoshimoto K, Hanaoka H, Sato S, Kato T, Tabata S, Noda T, Ohsumi Y (2004) Processing of ATG8s, ubiquitin-like proteins, and their deconjugation by ATG4s are essential for plant autophagy. Plant Cell 16: 2967-2983.
Google Scholar: Author Only Title Only Author and Title

Yu Z-Q, Ni T, Hong B, Wang H-Y, Jiang F-J, Zou S, Chen Y, Zheng X-L, Klionsky DJ, Liang Y (2012) Dual roles of Atg8–PE deconjugation by Atg4 in autophagy. Autophagy 8: 883-892.
Google Scholar: Author Only Title Only Author and Title

Zaffagnini M, Fermani S, Marchand CH, Costa A, Sparla F, Rouhier N, Geigenberger P, Lemaire SD, Trost P (2019) Redox Homeostasis in Photosynthetic Organisms: Novel and Established Thiol-Based Molecular Mechanisms. Antioxid Redox Signal 31: 155-210.
Google Scholar: Author Only Title Only Author and Title

Zheng X, Yang Z, Gu Q, Xia F, Fu Y, Liu P, Yin XM, Li M (2020) The protease activity of human ATG4B is regulated by reversible oxidative modification. Autophagy: 1-13.

Google Scholar: Author Only Title Only Author and Title